RESEARCH ARTICLE

Basin Research | IAS EAGE WILEY

Impact of faulting in depocentres development, facies assemblages, drainage patterns, and provenance in continental half-graben basins: An example from the Fanja Basin of Oman

Camilla L. Würtzen[1] | Alvar Braathen[1] | Miquel Poyatos-Moré[2] | Mark J. Mulrooney[1] | Lina H. Line[3] | Ivar Midtkandal[1]

[1]Department of Geosciences, University of Oslo, Oslo, Norway

[2]Departament de Geologia, Universitat Autònoma de Barcelona, Cerdanyola del Vallés, Spain

[3]Aker BP ASA, Lysaker, Norway

Correspondence
Camilla L. Würtzen, Department of Geosciences, University of Oslo, P.O. Box 1047, Blindern, N-031 Oslo, Norway.
Email: c.l.wurtzen@geo.uio.no

Abstract

Fault throw gradients create transverse folding, and this can influence accommodation creation and sedimentary routing and infill patterns in extensional half-graben basin. The Fanja half-graben basin (Oman) offers an excellent outcrop of an alluvial fan succession displaying cyclical stacking and basin-scale growth-fold patterns. These unique conditions allow for an investigation of fault-timing and accommodation development related to fault-transverse folding. Our study combines geological mapping, structural analysis, sedimentary logging and correlation, and bulk mineralogical compositions. Mapping reveals that the basin is bounded by a regional-scale fault, with local depocentres changing position in response to transverse syncline and anticline development ascribed to fault-displacement gradients. The alluvial Qahlah Formation (Late Cretaceous) is unconformably overlying the Semail Ophiolite, and is in turn overlain by the marine Jafnayn Formation (Late Palaeocene). Facies and stratigraphic analysis allows for subdivision of the Qahlah Formation into four informal units, from base to top: (i) laterite in topographic depressions of the ophiolite, (ii) greenish pebbly sandstones, deriving from axially draining braided streams deposited in the low-relief half-graben basin. This green Qahlah grades vertically into the red Qahlah, formed by alluvial fanglomerates and floodplain mudstones, with drainage patterns changing from fault-transverse to fault-parallel with increasing distance to the main fault. The red Qahlah can be divided into (iii) the Wadi al Theepa member, found in a western basin depocentre, with higher immaturity and sand: mud ratio, suggesting a more proximal source, and (iv) the Al Batah member, located in the eastern part of the basin. The latter shows better sorting, a lower sand: mud ratio, and more prominent graded sub-units. It also shows eastward expansion from an orthogonal monocline, ascribed to accommodation developed in a relay

ramp. Changes in sedimentary facies and depositional patterns are consistent with differential mineralogical composition. The Green Qahlah is composed of quartz and lithic mafic rock fragments, sourced from the ophiolite and schists of the metamorphic basement. The Red Qahlah is composed of chert and kaolinite sourced from the Hawasina Nappe succession in the footwall of the master fault. These changes in source area are linked to unroofing of fault-footwalls and domal structures during the extensional collapse of the Semail Ophiolite. The novelty of this study resides in linking sedimentology and fault-displacement events controlling fault-perpendicular folding, and its influence on depocentre generation and stratigraphic architecture. This is an approach seldom considered in seismic analysis, and rarely analysed in outcrop studies, thus placing the results from this study among the key outcrop-based contributions to the field.

KEYWORDS

alluvial sedimentary infill, continental half-graben basin, depocentre development, Fanja Basin, fault-transverse folding, Oman, provenance shift, Qahlah formation, sedimentary routing, syn-rift

1 | INTRODUCTION

Fault-bound extensional basins are sensitive to fault-displacement development, since extensional faulting and related folding exert a control on the location, shape and size of sedimentary basins, and the distribution, thickness and preservation of the sediments filling them (Friedmann & Burbank, 1995; Gawthorpe & Leeder, 2000; Schlische, 1995; Schlische et al., 1996; Serck & Braathen, 2019). Such basins are very common in the geological record, and often host abundant natural resources in the subsurface. Accordingly, their architecture has been extensively studied, and our current understanding of rift basins resides in a toolbox of well-constrained models, hinged on combinations of seismic analysis supported by well data, and outcrop studies. These span from fault-growth models (e.g. Rotevatn et al., 2019; Walsh et al., 1998), to models of fault-controlled catchment systems and their sedimentary sinks (e.g. Gawthorpe & Leeder, 2000; Leeder & Gawthorpe, 1987).

The production and availability of sediments infilling extensional basins, particularly in continental examples, are highly dependent on catchment bedrock lithology (Blair, 1999b; Levson & Rutter, 2000) as well as climate, which control precipitation and weathering, both within the basin and in catchment areas (Nystuen et al., 2014). As such, alluvial fan systems are highly sensitive recorders of tectonic movements, provenance changes and climate (Blair, 1987; Harvey et al., 2005). However, establishing a general model for alluvial fan deposition considering several controls (i.e. tectonic, climatic, provenance,

Highlights

- The Fanja Basin infill reveal facies variations and architectural changes, verifying fault-orthogonal folding.
- Depocentre migration, enhanced by climatic fluctuations, controlled facies distribution and sand:mud ratio.
- Cyclical stacked alluvial conglomerate and mudstone reflects fan advance and -retreat induced by varying A/S rates.
- Palaeo-drainage trends reflect a shift from axial during early rifting to fault-transverse in the rift climax.
- Mineralogical changes suggest a provenance shift caused by changing basin configuration and footwall unroofing.

and base-level) has caused difficulty and controversy (Lecce, 1990). To some extent, classical conceptual models may be biased towards examples from arid conditions (e.g. Blair, 1999a, 1999b, 1999c, 2000; Brooke et al., 2018; Clarke, 2015; Parker, 1999), although they develop in all climatic belts (e.g. De Haas et al., 2015; Mather et al., 2017; Nott et al., 2001; Saito & Oguchi, 2005). Furthermore, catchment lithology and precipitation patterns also control alluvial depositional processes, which range from gravity to hyperconcentrated and sheet flows, to channelised stream flows and aeolian reworking (Calhoun & Clague, 2018; Ghinassi & Lelpi, 2018; Jo et al., 1997; Moscariello, 2018;

North & Davidson, 2012; Ridgway & Decelles, 1993; Sohn et al., 1999). Another misconception concerns the general assumption of overall coarsening-upwards alluvial fan succession profiles (e.g. Lin et al., 2022; Mack & Rasmussen, 1984; Steel et al., 1977; Steel & Ryseth, 1990). Alluvial fan deposits frequently aggrade in their proximal environments (Evans, 1991; Harvey, 1997), and the onset of fan deposition is often abrupt compared with the following abandonment, which may happen gradually, forming fining-upwards profiles (e.g. Mack & Leeder, 1999).

In order to further understand the formation and development of continental rift basins and how their structural control affect sedimentary architecture, the Fanja half-graben basin in the Al Hajar Mountain, NE Oman (Figure 1), is analysed by combining sedimentary interpretations and correlations, bulk mineralogical compositions and structural geometries. The Fanja Basin offers a unique outcrop of a Late Cretaceous tropical alluvial fan succession displaying a cyclical stacking and basin-scale growth-fold patterns allowing for investigation of fault-timing and accommodation development related to fault-transverse folding. To be able to predict the heterogeneities in stratigraphy and sedimentology in fault-influenced basins, it is important to understand how faults grow and what the basin-geometric effects of this are besides the sedimentary response to varying accommodation. Important models for the growth and infill of fault-bounded basins, like those of Schlische (1995), Schlische et al. (1996), Gawthorpe and Leeder (2000), Peacock and Sanderson (1994), and Prosser (1993), just to mention some, have paved the way for this field of research. However, these articles are mostly conceptual. The novelty of our study resides in the outcrop example forming the study case: the reasonable size, good exposure and high degree of preservation enables analysis of the distribution of facies in continental deposits in close connection with faults. The link between sedimentology and fault-displacement events controlling fault-perpendicular (orthogonal) folding offers spatial control on depocentres and thereby depositional loci. This is an approach only recently considered in seismic analysis (e.g. Serck & Braathen, 2019), but rarely analysed in outcrop studies, which increases the potential application of this study to subsurface reconstructions.
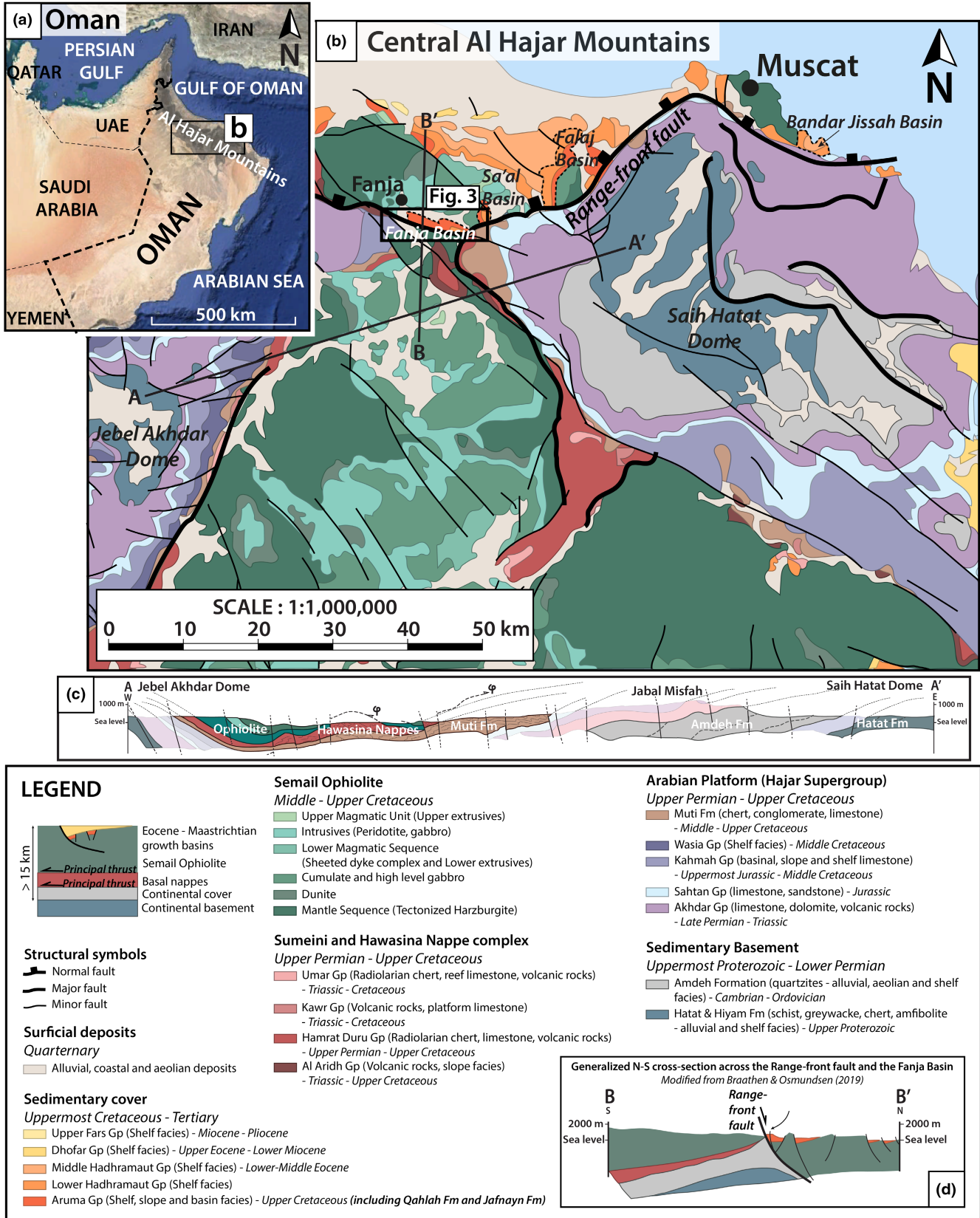
2 | GEOLOGY AND STRATIGRAPHY

2.1 | Basin setting

The principal structure of the studied basin is the regional range-front fault (Braathen & Osmundsen, 2019; Mattern

& Scharf, 2018). This steeply north-dipping extensional fault shows km-scale extensional offset of the Semail ophiolite, with the Fanja half-graben situated to its northern hanging wall (Figure 1). The Fanja Basin forms part of an array of preserved basins in the hanging-wall to the range-front fault, e.g. the Sa'al, Falaj and Bandar Jissah basins as shown in Figure 1 (Alsharhan & Nasir, 1996; Serck et al., 2021). Recent work addressing extensional collapse of the ophiolite adds new perspectives on the overlying fault-bound basins (Braathen & Osmundsen, 2019; Serck et al., 2021). For example, Serck et al. (2021) have highlighted the interaction of a low-angle extensional detachment and steep normal faulting impacting the sedimentary infill of the Bandar Jissah Basin along the hanging-wall of the same regional fault that bound the Fanja Basin, suggesting similar tectonic histories.

The Al Hajar Mountains of northern Oman feature a world-class example of an ophiolite complex (e.g. Searle, 2019; Searle & Cox, 1999) and accordingly, significant attention has been directed to the Semail Ophiolite, which forms the uppermost unit above a stack of continental margin nappes. Regional tectonostratigraphy spans Precambrian and Permian to Upper Cretaceous rocks, which are either autochthonous below the nappes or obducted onto the Arabian Neo-Tethys margin in the Late Cretaceous as allochthonous units (Cooper et al., 2014; Searle, 2007, 2019). During final south to SSE emplacement of the ophiolite, in the Campanian to Maastrichtian stages of the Late Cretaceous, extensional faulting started influencing the region, leading to a long-lived phase of extensional collapse of the ophiolite with substratum (Braathen & Osmundsen, 2019; Serck et al., 2021), lasting at least to the Late Eocene as manifested by for instance the Range-front fault. Initial Maastrichtian basins, including the Fanja Basin, were mainly continental (Searle & Cox, 1999) prior to regional uplift and erosion, followed by regional subsidence and marine transgression in the Late Palaeocene (Braathen & Osmundsen, 2019) progressing to an Eocene marine carbonate platform with localised faulting (e.g. Serck et al., 2021). Regionally, extension is demonstrated by wide-spread normal faulting above major extensional detachments, with significant extension unroofing deeper units including eclogites from the former subduction zone, as manifested at the surface by the Jebel Akhdar and Saih Hatat domes. Unroofing was fast and nearly isothermal, a common trait of extensional collapse (e.g. Brun et al., 2018), starting in the Maastrichtian and ending in the Eocene (Hansman et al., 2017). In current map-view, these domes encompass (1) Precambrian (sedimentary) basement (e.g. Hatat and Amdeh formations), and (2) Middle Permian to Cenomanian shelf-carbonates (e.g. Muti Formation), bound by (3) Late Permian to Late Cretaceous Tethyan oceanic sediments of the Sumeini and

(a) Oman

PERSIAN GULF
IRAN
QATAR
GULF OF OMAN
UAE
Al Hajar Mountains
b
SAUDI ARABIA
OMAN
ARABIAN SEA
YEMEN

500 km

(b) Central Al Hajar Mountains

Muscat

B'
Fakai Basin
Fanja
Sa'al Basin
Fig. 3
Range-front fault
Bandar Jissah Basin

Fanja Basin
A'
Saih Hatat Dome
B
A
Jebel Akhdar Dome

SCALE : 1:1,000,000
0 10 20 30 40 50 km

(c)
A W Jebel Akhdar Dome
1000 m
Sea level
Ophiolite Hawasina Nappes Muti Fm
Jabal Misfah
Saih Hatat Dome A' E
Amdeh Fm Hatat Fm
1000 m
Sea level

LEGEND

Eocene - Maastrichtian growth basins
Semail Ophiolite
Principal thrust
Basal nappes
Principal thrust
Continental cover
Continental basement

Structural symbols
Normal fault
Major fault
Minor fault

Surficial deposits
Quarternary
Alluvial, coastal and aeolian deposits

Sedimentary cover
Uppermost Cretaceous - Tertiary
Upper Fars Gp (Shelf facies) - *Miocene - Pliocene*
Dhofar Gp (Shelf facies) - *Upper Eocene - Lower Miocene*
Middle Hadhramaut Gp (Shelf facies) - *Lower-Middle Eocene*
Lower Hadhramaut Gp (Shelf facies)
Aruma Gp (Shelf, slope and basin facies) - *Upper Cretaceous (including Qahlah Fm and Jafnayn Fm)*

Semail Ophiolite
Middle - Upper Cretaceous
Upper Magmatic Unit (Upper extrusives)
Intrusives (Peridotite, gabbro)
Lower Magmatic Sequence (Sheeted dyke complex and Lower extrusives)
Cumulate and high level gabbro
Dunite
Mantle Sequence (Tectonized Harzburgite)

Sumeini and Hawasina Nappe complex
Upper Permian - Upper Cretaceous
Umar Gp (Radiolarian chert, reef limestone, volcanic rocks) - *Triassic - Cretaceous*
Kawr Gp (Volcanic rocks, platform limestone) - *Triassic - Cretaceous*
Hamrat Duru Gp (Radiolarian chert, limestone, volcanic rocks) - *Upper Permian - Upper Cretaceous*
Al Aridh Gp (Volcanic rocks, slope facies) - *Triassic - Upper Cretaceous*

Arabian Platform (Hajar Supergroup)
Upper Permian - Upper Cretaceous
Muti Fm (chert, conglomerate, limestone) - *Middle - Upper Cretaceous*
Wasia Gp (Shelf facies) - *Middle Cretaceous*
Kahmah Gp (basinal, slope and shelf limestone) - *Uppermost Jurassic - Middle Cretaceous*
Sahtan Gp (limestone, sandstone) - *Jurassic*
Akhdar Gp (limestone, dolomite, volcanic rocks) - *Late Permian - Triassic*

Sedimentary Basement
Uppermost Proterozoic - Lower Permian
Amdeh Formation (quartzites - alluvial, aeolian and shelf facies) - *Cambrian - Ordovician*
Hatat & Hiyam Fm (schist, greywacke, chert, amfibolite - alluvial and shelf facies) - *Upper Proterozoic*

Generalized N-S cross-section across the Range-front fault and the Fanja Basin
Modified from Braathen & Osmundsen (2019)
B S
Range-front fault
B' N
2000 m
Sea level
2000 m
Sea level
(d)

Hawasina nappe complex, and (4) the Semail Ophiolite (Figure 2; Searle, 2007). These units are potential source terranes for sediments when provenance of basin-fill is examined, substantiating descriptions. There is limited work addressing the sediments deposited after the obduction of the ophiolite (e.g. Abdelghany, 2006; Alsharhan

FIGURE 1 (a) Overview map of the SE Arabian peninsula with inset box showing the location of the (b) geological map of the central Al Hajar Mountains of NE Oman (legend for explanation) with the main structural elements and referenced Maastrichtian-Eocene extensional basins labelled. Locations of cross-section (c) and (d) are marked on the figure as well as the location for Figure 3. (c) WSW-ENE cross-section across the two domal structures Jebel Akhdar and Saih Hatat. Map (b) and cross-section (c) is modified from published map of Fanja region (Villey et al., 1986) for the Oman Ministry of Petroleum and Minerals. (d) N-S fault-transverse cross-section across the range-front fault displaying the relation between the ophiolite and underlying nappe structures in the footwall and the extensional basins (including the Fanja Basin) in the hanging-wall (modified from Braathen & Osmundsen, 2019).

& Nasir, 1996; Nolan et al., 1990). Especially, the Fanja Basin succession has only been studied in one publication (Abbasi et al., 2014).

2.2 | Stratigraphy, palaeoclimate and palaeogeography

During the Late Cretaceous to Palaeogene, northern Oman formed an emerged peninsula in the Tethys Ocean (Nolan et al., 1990), located at an equatorial position (Matthews et al., 2016). A regional unconformity truncates all allochthonous units throughout Oman and the UAE Mountains. Above the unconformity, conglomerates and shales of the Qahlah Formation and Al Khawd Formation, the latter a south-eastern equivalent (Nolan et al., 1990) are overlain by a transgressive sequence of progradational sandstones and marls and shallow marine limestones of the Simsima (Late Maastichtian) and Jafnayn (Late Palaeocene) formations, followed by open-marine carbonate platform deposits of the Seeb Formation (Early Eocene). The Palaeocene-Eocene succession topping the Fanja Basin are, however, outside the scope of this study, as we address the coarse continental fill of the Maastrichtian Qahlah Formation.

In the Fanja Basin (and common elsewhere), the first autochthonous deposits onto the exhumed ophiolite surface are lateritic ferruginous clay- and siltstones (5–20 m thickness) of the basal Qahlah Formation (Alsharhan & Nasir, 1996). Where preserved, laterite has a gradational contact into the underlying pristine ophiolite. Laterites appear in depressions of the low-relief ophiolite surface, providing a strong indicator of the tropical humid climate, which dominated during the Cretaceous in the region (de Winter et al., 2017; Huber et al., 2002). The Qahlah Formation varies significantly in stratigraphic expression and thickness between basins, exhibiting mainly interior continental alluvial sediments. Coastal and shallow marine fan-deltas and carbonate build-ups have been ascribed to the Al Khawd Formation in the southern foreland of the thrust stack (Nolan et al., 1990); however, similar deposits in the Oman mountains are sporadic and appear placed in the Simsima Formation overlying the Qahlah Formation. In any case, such heterogeneity is common

to basal terrigenous sediments directly overlying an unconformity and express the Late Cretaceous palaeogeographical setting of the northern Oman peninsula with a continental interior and a surrounding coastal environment (Nolan et al., 1990).

2.3 | Fanja Basin configuration

As mentioned, the Fanja Basin forms an elongated, east–west striking half-graben in the hanging-wall of the Range-front fault, located to an along-fault syncline with a gently south-dipping to sub-horizontal northern flank and a steeper southern flank up towards the fault (Figure 3a,b). The first-order fault consists of several curvilinear segments (Figure 3a), with two segments converging in a noticeable jog along the eastern basin boundary. Further, a smaller jog central to the basin suggests linkage of segments in this area. These two linkage areas, or breached relays (Peacock & Sanderson, 1994; Rotevatn et al., 2007), indicate the presence here of fault-perpendicular (orthogonal) anticlines (Figure 3a) inherited from fault-displacement gradients (e.g. Serck & Braathen, 2019). Similarly, areas of larger fault-throw host orthogonal synclines, which is particularly striking in the eastern part of the basin (Figure 3a). These folds are reflected in both thicknesses and facies-belt distributions of the basin succession, which further constrain their timing and propagation. In addition, there are numerous steep, extensional faults impacting the basin-fill, of which those of greater extend and throw tend to be subparallel to the Range-front fault, as shown in Figure 3a,b, and described below. These faults control growth-sections on the metre (m) to 10-m scale, substantiating that active faulting created accommodation in the basin during deposition.

Preserved stratigraphy in the Fanja basin starts with the widespread Maastrichtian Qahlah Formation, overlain by the Late Palaeocene Jafnayn Formation, the latter only preserved in the east (Figures 2 and 6). The Qahlah Formation consists at its base of isolated occurrences of a few metres of laterite (the *Laterite member*) overlain by up to 35 m of green fluvial sandstones and conglomerates of the *Green Qahlah member*, thickest in the east at Al Batah and in the immediate hanging-wall to the Range-front fault in Fault Valley (Figure 3d). The Green Qahlah member is conformably
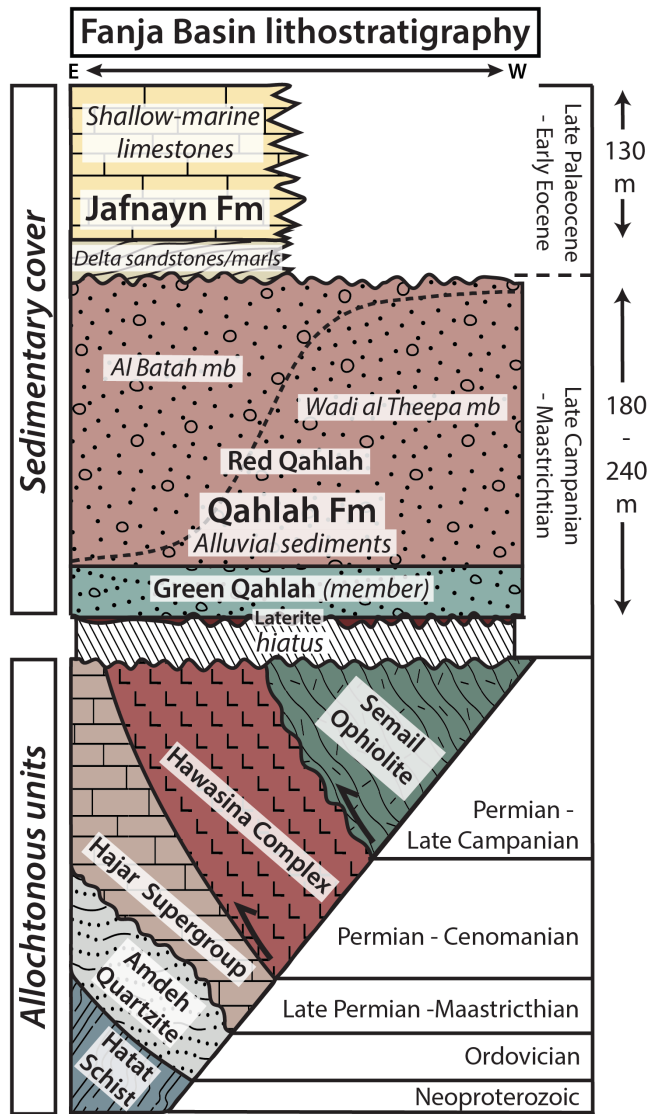
FIGURE 2 E-W lithostratigraphic chart for the Neoproterozoic-late Campanian overall allochthonous units and overlying late Campanian-early Eocene sedimentary cover in the Fanja Basin. The oblique arrangement of the allochthonous units illustrates the stacking of nappes induced by ophiolite obduction with an exhumed, erosional surface and hiatus between these and the post-obduction sedimentary depositional sequence. The nomenclature for the allochthonous units is in accordance with the scheme applied in Braathen and Osmundsen (2019) and published bedrock maps (Villey et al., 1986) for the Oman Ministry of Petroleum and Minerals. The Qahlah Formation and Jafnayn Formation are official accepted nomenclature; however, the internal subdivision into members is suggested here in this paper for the first time based on observations from this work.

overlain by 35–210 m thick cyclically interbedded orange-red alluvial conglomerates and red floodplain mudstone of the Red Qahlah members (Figure 3c). Of these, the *Wadi al Theepa member* (lower Red Qahlah) is thickest in the western basin and thins towards the central part, whereas the *Al*

Batah member (upper Red Qahlah) fills the basin in the east around the synclinal structure expressed orthogonal to the major fault-jog (Figure 3a,d). In the eastern basin, the Qahlah Formation is capped by a transgressive lag of the Jafnayn Formation, either an oyster-bed (Al Batah) or a beach conglomerate (near cross-road). This lag is overlain by up to 50 m of deltaic sandstone and marl and finally capped by 90 m of shallow marine ramp carbonates (Olaussen, Midtkandal and Stemmerik, pers. com. 2020).

3 | DATA AND METHODS

3.1 | Fieldwork and sedimentological analysis

Data for this study were collected during two field seasons in 2020 and 2022, respectively. Fieldwork was carried out conventionally by mapping of the basin with collection of structural data, and logging of sedimentological sections in scale 1:200. The latter emphasises grain size variations, sedimentary structures, architectural elements, and palaeocurrent indicators. About 157 palaeocurrent (PC) measurements were obtained in the Green Qahlah member and 111 PC measurements in the Red Qahlah member interval distributed between eight measuring points (Figure 3a). PC measurements were corrected to dip of beds and plotted using GeoRose 0.5.1 software, whereas fault orientations are plotted in Move. With overall gentle dips of bedding in the basin, PC and fault orientations are plotted as recorded. A dataset consisting of photographs and high-resolution photomosaics and field-sketches were applied in the analysis of facies, architecture and structural influence on cm to km-scale. Several facies were defined representing depositional processes (Table 1). These were further divided into associations representing depositional environments (Table 2).

3.2 | Mineralogical petrography

Sampling throughout the Qahlah Formation succession was conducted for petrographic analysis with the intention of tracing the sediment source and possible changes in this, which is already indicated on a sedimentary scale by the change in colour and clast-type up through the succession. This analysis was anticipated to reveal any link in mineralogical compositional changes to changes in facies, and in fault-intensity. Twenty samples collected from the Qahlah Formation were included in this study, 17 from sandy fluvial to alluvial (channel-, splay- and fan-) facies and three floodplain mudstone samples. Samples were
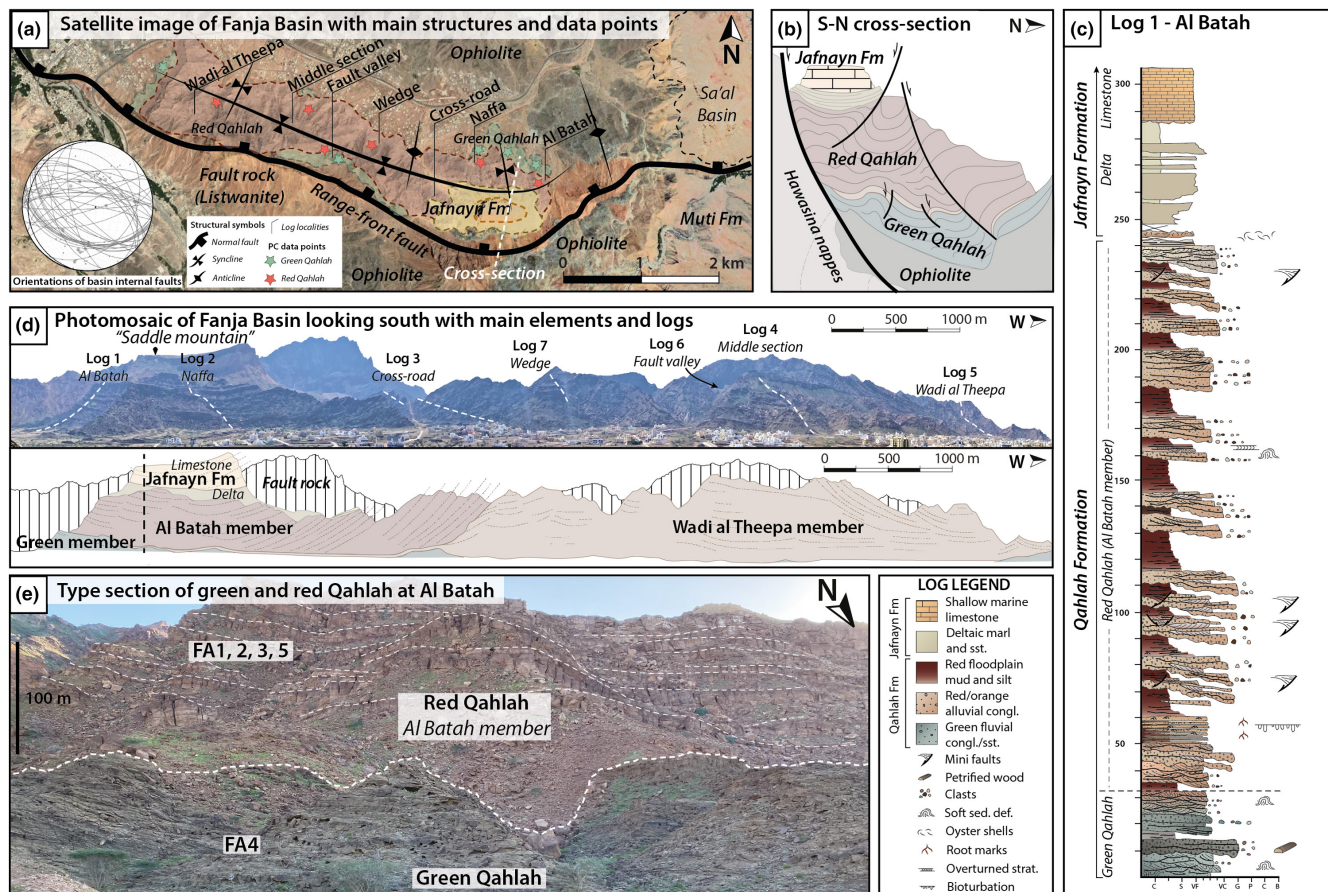
FIGURE 3 (a) Satellite image of the Fanja Basin and western Sa'al basin with main geological units and structural elements. The location of cross-section (b) and logged sections is marked and labelled as well as locations for palaeocurrent measurements marked with a star (green for green Qahlah and red for red Qahlah members). The stereoplot displays orientations of basin internal faults in the Fanja Basin. (b) S-N cross-section through the eastern Fanja Basin showing the relations between internal sedimentary units and basin internal faults to the range-front fault and allochthonous units in footwall and hanging-wall. (c) Key sedimentary log from Al Batah displaying the green Qahlah member and Al Batah member of the Qahlah Formation and overlying deltaic and limestone shelf deposits of the Jafnayn Formation with key sedimentary features (see legend for explanation). (d) E-W photomosaic of the Fanja Basin outcrop with log-locations (upper) and the interpreted section (below) with main stratigraphic units, bedding geometries and the location of cross-section (b). (e) Type section at Al Batah showing the green Qahlah member and Al Batah member and the relation between the two. Bedding boundaries (tops of conglomeratic beds) in the Al Batah member are marked together with main facies associations characteristic to the two members.

collected at every 20–40 m interval through the succession with closer sampling over the transitional interval from Green to Red Qahlah. Fourteen samples are from the eastern basin at Al Batah and Naffa and three samples are from the western basin at Wadi al Theepa.

3.2.1 | XRD bulk analysis

The 17 sandy samples were analysed with conventional powder X-ray diffraction (XRD) using a D8 Bruker Powder X-ray diffractometer. Identification and relative quantification of mineral phases were modelled and analysed by Rietveld refinement through the software BGMN-Profex (version 4.3.1). With XRD results, the average mineral

composition was established, and sandstones were classified according to a QRF plot diagram. The XRD results interpretation is summarised in Figure 4.

Of the three mudstone samples, two were sampled from the Red Qahlah members and one from the Green Qahlah. Due to the complexity in the structures of clay minerals, quantitative measurements of specific clay phase abundances were treated and analysed separately from the bulk.

3.2.2 | Elemental distribution analysis (SEM)

Thin sections of the 17 sandy samples were prepared at the Department of Geosciences (University of Oslo) for analysis of mineralogical and textural characteristics. Monogranular

TABLE 1 Summary of 21 lithofacies (A–U) observed in the Fanja Basin with representative pictures, descriptions of lithology, texture and sedimentary structures, and the depositional processes inferred from these. The lithofacies are combined into facies associations 1–8 summarised in the right-hand side

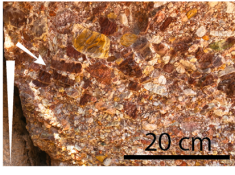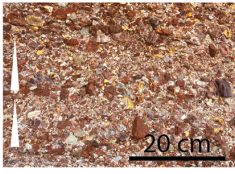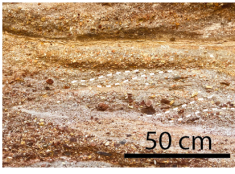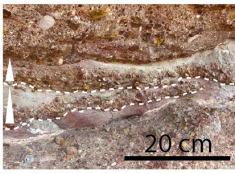**TABLE 1.1** Facies description and inferred depositional processes
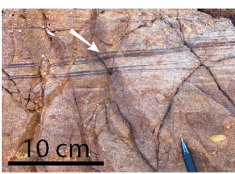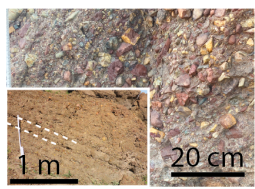
Code	Picture	Lithology and texture	Sedimentary structures	Depositional process	Facies association	
A		Pale orange-pink to pale-red or green-grey conglomerate (very coarse sand to cobble grade); clast-supported (less commonly matrix-supported); polymict; poorly-sorted; sub-angular to sub-rounded clasts	Ungraded to inverse graded; A-axis imbrication (arrowed); outsized clasts; 10-100 cm thick beds with gradational boundaries or occuring as small clusters; transitional lower contact (except when overlaying mudstone)	Gravelly (low-viscous), diluted debris flows (Collinson, 2006; Miall, 2010)	1	*Gravel-rich hyperconcentrated flow deposits* — Sequence of interchanging facies A, B, and C with transitional, diffuse boundaries and interbedded facies D together represent hyperconcentrated flows in the transitional regime between gravity (turbulent) flow and fluvial bedload (Siegenthaler & uggenberger, 1993)
B		Pale orange-pink conglomerate (granule to pebble grade); clast-supported; polymict; moderate/poorly-sorted; sub-angular to sub-rounded	Ungraded to normal graded (marked); random or flat clast orientation; 10-150 cm thick beds, often repetitive in several meter thick sequences; transitional to sharp lower contact	Pseudoclastic, diluted flash floods or traction carpets deposited through traction currents into turbulent suspension (Nemec & Steel, 1984; Nemec & Muszynsk, 1984; Collinson, 2006)		
C		Pale orange-pink to grey-yellow conglomerate (very coarse sand to pebble grade); clast-supported; polymict; moderate/poorly-sorted; sub-rounded clasts	Massive or normal graded; structureless to sporadic crude horizontal to low-angled cross-stratification with clasts lining foresets (marked), preferably in upper part; transitional to sharp lower contact	Bedload transport into turbulent suspension in upper-(horizontal stratification) to lower (cross-stratification) flow-regime through migration of coarse-grained bars in mid-fan channels (Nemec & Muszynski, 1984; Sohn et al., 1999)	2	*Mixed gravel- to sand-rich stream flow deposits* — Facies A and B together dominated the inner fan zone, wheres as facies B, C, and D dominate the medial fan zone
D		Pale grey-pink to white (sharp colour transitions) fine- to medium-grained pebbly sandstone; moderate/well-sorted	Normal graded (marked) lenticular beds (0,1-0,5 m thick) with clast (granule to pebble grade) interlayers in scour clusters (marked) or as coarse tails; horizontal to low-angle cross-stratification with clast-alignment on foresets (imbrication); sharp surrounding contacts	Stream-flow deposition (good sorting, grain-size separation, localization of scours) through short-lived bedload traction currents (Sohn, 1997; Dasgupta, 2006)		
E		Pale red to grey-orange medium-grained pebbly sandstone; moderate sorted	Diffuse horizontal- to low-angle cross-lamination; dark-draping on foresets (arrowed) with increasing angle of climb; sporadic clasts (granule to pebble grade); transitional surrounding contacts; lense-shaped bed geometry	Sub-aqueous upper flow-regime flat beds into lower flow-regime migration of straight-crested dunes and ripples with high sediment load	3	*Sand-rich flash flood and minor stream deposits* — Shallow stream deposition (E, H) in the scoured fan-surface with bank/bar/levée collapse (F, G) during high sediment loads under flashy-discharge or during syn-depositional disturbance (Jones & Rust, 1983; Horn et al., 2018)
F		Pale grey-orange to pale green fine- to medium grained sandstone; well-sorted	Convolute bedding; tabular bed geometry (0,2-1 m) with sharp lower boundaries to conglomeratic facies (marked), and gradational upper boundaries	Disruption of liquified sediment layering (Collinson, 2006)		
G		Pale grey-orange or pale green fine-grained sandstone; well-sorted	Overturned/recumbent cross-bedding (marked); multiple 10-20 cm bedsets	Shearing of upper part of tabular cross-beds (subaqueous migrating sinuous-crested dunes in lower flow-regime) by overriding currents. Caused by fluctuations in flow conditions and (high) sediment load (Stikes, 2007)		
H		Pale grey-pink to yellow-white, fine-grained sandstone; well-sorted	Low-angled cross-lamination (sub-critical; marked) in otherwise structureless to crudely thinly (cm) bedded matrix	Sub-aqueous migration of ripples and small dune-bedforms in lower flow-regime		

TABLE 1 (Continued)

TABLE 1.2. Facies description and inferred depositional processes

Code	Picture	Lithology and texture	Sedimentary structures	Depositional process	Facies association	
I	50 cm	Pale orange-pink or pale grey-green fine- to medium-grained sandstone; moderate/well-sorted	Structureless or crudely laminated with sporadic clusters of clasts or floating clasts (granule grade); erosional lower contact	Rapid deposition in high sediment load, preventing bedform development. Minor tractional processes (gravel lags) (Miall & Jones, 2003; Horn et al., 2018)	**4** *Sand-rich braided stream deposits*	Based on grain size, amalgamation, structures, and lack of preserved overbank deposits, the facies are inferred to represent a shallow braided stream system (Nichols & Fisher, 2007) with locally well-developed subaqueous dune-fields (K) (Sadler & Kelly, 1993), interchannel bars (L) and channel base lags, and aggradational low-relief longitudinal bars (J) (Jo et al., 1997; Miall, 1997a,b; Rust, 1978; Puy-Alquiza et al., 2017). The mature state indicated a distal sediment-source
J	1 m 20 cm	Dusky dark grey-green to orange conglomerate (very coarse sand to cobble grade); clast- to matrix-supported (varying bands); polymict; moderate/poorly-sorted; sub-rounded	Ungraded; flat clast orientation; tabular bed-geometry; horizontal to low-angle bedding (marked) (5-15 cm bedsets in 15-500 cm thick beds); flat clast orientation; sharp lower contact	Gravel sheet deposited as bedload or traction carpets (Hein & Walker, 1977; Ashmore, 1985; Reid & Frostick, 1986; Whiting et al., 1988; Jo et al., 1997; Suresh et al., 2007; Calhoun & Clague, 2018)		
K	20 cm	Pale green to gray-orange medium- to coarse-grained sandstone and gravel; well-sorted	Trough-cross bedding (marked) with basal lags (granule to pebble grade); normal grading; single- (tens of cm) or multiple sets (50-100 cm); reactivation surfaces	Sub-aqueous migration of sinuous-crested dunes in the lower flow-regime of channels (Hjellbakk, 1997; Collinson, 2006)		
L	20 cm	Pale green to gray-orange medium- to coarse-grained sandstone; well-sorted	Planar cross-bedding with normal grading; single- or multiple sets (20-100 cm); reactivation surfaces; sporadic clasts on foresets and mud-draping	Sub-aqueous migration of straight-crested dunes in the lower flow-regime or deposition off the distal end of intra-channel bars in the upper flow-regime (Hjellbakk, 1997; Collinson, 2006)		
M	20 cm 2 m	Pale orange-pink fine- to medium-grained sandstone; moderate sorted	Structureless; crudely accreting bed-sets (marked); wedge-shaped geometry with sharp scouring bases; load-structures into underlying mudstone (marked)	Rapid sedimentation where sand is loaded through crevasse splays onto waterlogged mudstones of floodplains (Gulliford et al., 2017). Accretion may be caused by sidebar growth (Collinson, 2006)	**5** *Heterolithic overbank deposits*	Prograding depositional bodies of sand onto floodplain mudstones (crevasse splay) or into lakes (lacustrine delta) (Renaut & Gierlowski-Kordesch, 2003; Gulliford et al., 2017)
N	10 cm 20 cm	Heterolithic yellow-brown to purple-red very fine-grained sandstone and yellowish-white to reddish-brown siltstone and mudstone	Thinly interbedded heterolithic units; overall coarsening and thickening upwards; asymmetric and symmetric ripple cross-lamination; dark red rootlets; horizontal tube-shaped "meander" bioturbation traces (*Gordia Marina isp.*, pers. com.; arrowed)	Crevasse splay or lacustrine deltaic deposition. Interchanging suspension fallout (silt) and stream-flow (sand). Combined flow-ripple migration dominated by unidirectional currents (stream-flow with a wave component; Collinson, 2006). Progradation causing upwards-coarsening.		

(Continues)

grains (e.g. quartz, K-feldspars, micas) are distinguished from polygranular grains (e.g. microcrystalline chert, igneous/volcanic rock fragments, mica schist and sedimentary mudrock fragments). Recrystallised framework grains (pseudomorphous replacements) and completely dissolved particles (secondary porosity) are treated as part of the rock fragment assembly. The relative amount of allogenic matrix, authigenic cements (e.g. quartz, chlorite, kaolinite, illite and various carbonate minerals) and intergranular porosity defines the intergranular volume (IGV) of the sample. The thin sections were analysed through microscopy point counting (in plane- and cross-polarised light) combined with SEM scans to map the elemental distributions in the samples. The thin section interpretations are summarised in Figure 5.

TABLE 1 (Continued)

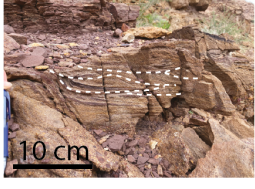**Table 1.3.** Facies description and inferred depositional processes
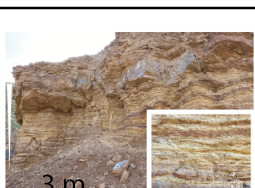
Code	Picture	Lithology and texture	Sedimentary structures	Depositional process	Facies association
O		Red-brown very fine- to fine-grained sandstone to medium-grained pebbly sandstone; moderate/well-sorted	Thin (5-20 cm) sheets often in mulitple sets; horizontal-, low-angle cross lamination or trough-cross stratification (marked) into ripple cross-lamination	Shallow sheet stream-flows	**6** *Fine-grained floodplain deposits* — Deposition at wet floodplain through suspension settling (P, Q) at interchannel mudflats and lacustrine environments with overbank spills and shallow streams (O). Typical for outer fan/fan fringe zone or adjacent to active fan. The inactive fan areas may experience non-deposition for longer time intervals with exposed surfaces where hard pans form
P		Red-brown mottled (white to okker-coloured) very fine- to fine-grained sandstone and siltstone	Structureless to faint undulating laminations	Suspension fallout with secondary migration of ripple-scale bedforms; mottled horizons represent kaolinitic soils	
Q		Dark red-brown to purple silt and mudstone; sporadic ochre-coloured mottling in horizons or stains (Rhizoliths; arrowed)	Honogeneous, structureless or with faint laminations; thick (up to 20 m) intervals between conglomeratic facies units or in faulted depressions in tops of these with growth features; concreted horisons; thin silt beds with ripple marks	Suspension faullout of clay particles. Mottled rhizoliths indicate pedogenesis and low sedimentation rates (Ridgeway & Decelles, 1993; Sønderholm & Tirsgaard, 1998; Schieber, 1999; Kraus, 1999; Hampton & Horton, 2007; Zhang et al., 2021)	
R		Orange to red-brown ironized siltstone	3-10 cm thick hard horizons on top of conglomerate beds (marked); may contain granule grade basal clasts and exhibit normal grading; sharp boundaries; tabular or filling cracks and scours	Oxisols formed by oxidation and precipitation of ferric iron oxides in alluvial gravel (i.e. hardpans; Blair & McPherson, 2009). Equivalent to lateritic soils forming on the ophiolite.	
S		Grey oyster shells in yellow-orange silty cement; poorly sorted	Structureless; chaotic distribution of oyster shells; 0,5 m thick; restricted to top of Qahlah Fm in Al Batah	Wave reworked oyster bank	**7** Pebbly beaches, possibly at fan-fringes, with significant wave action. Represent transgressive surfaces
T		Purple-grey fine- to medium-grained pebbly sandstone; moderate/well-sorted	Low-angled cross-stratification (marked) with clast alignment on foresets; tabular geometry; sharp boundaries; 0,3-0,5 m thick; only observed on top of Qahlah Fm at cross-road section	Deposition by wave reworking	
U		Yellow-red silt to fine-grained sand and greenish marls; well-sorted	Thinly interbedded overall repetitive coarsening- and thickening upwards (marked) units arranged in a larger scale coarsening upwards succession; wave ripples, cross-bedding; observed only in the eastern part of the basin	Prograding marine deposition	**8** Prodelta to delta front of shallow-water delta

TABLE 2 Summary of facies associations, their characteristic processes, main architectural elements and lithofacies, with an illustrative depiction of the elements in a conceptualised depositional model

FA1	FA2	FA3	FA4	FA5	FA6
Processes: Gravity to hyperconcentrated flow regime	Processes: Hyperconcentrated to stream flow regime with minor gravity flows	Processes: Stream flow regime with minor hyperconcentrated flows	Processes: Stream flow regime (bedload and traction currents)	Processes: Splay of sand onto floodplain, stream to sheet flow	Processes: Suspension fallout and minor stream and sheet flow
Elements: Debrites and massive conglomerates	Elements: Massive to stratified conglomerates and sandstones	Elements: Stratified gravel of minor (ephemeral) channels and sand-sheets	Elements: Side- and interchannel bars, subaqueous dune-fields and basal lags of braided streams	Elements: Crevasse splays and lacustrine mini-deltas	Elements: Massive mudstone, soils, sand-lenses and -sheets of floodplain
Facies: A, B, (D)	Facies: (A), B, (C), D	Facies: (B), C, E, F, G, H, I	Facies: J, K, L, F, I, (A)	Facies: M, N, I	Facies: O, P, Q, R

4 | RESULTS

4.1 | Structural analysis: Outcrop geometry and fault patterns

As outlined above, the Fanja Basin exhibits an elongate, longitudinal syncline that parallels the Range-front fault (Figure 3). There are two transverse synclines and one transverse anticline perpendicularly intersecting the longitudinal syncline in the present-day outcrop geometry (Figure 3a,d). One of these transverse synclines correspond to a curvilinear portion of the Range-front fault towards the east of the basin (Al Batah). Pervasive faulting (1 to >10 m displacement) intersects all outcrops in the Fanja Basin and approximately parallels the Range-front fault's E-W to WNW-ESE strike (Figure 3a). Faults dip steeply NNE (synthetic) or SSW (antithetic), but dip angles of synthetic faults are more varied. Kinematic indicators (offset of beds and slickensides) conform to dip-slip, normal movements, especially by larger faults paralleling the Range-front fault. There is, however, faults that display a minor component of lateral movement (mostly sinistral), mainly proximal to the eastern jog in the Range-front fault. Several growth packages are recognised, especially in the Red Qahlah members where fine-grained facies fill hanging-wall accommodation above faulted, tabular conglomeratic sequences (Figure 6). With some small growth packages observed in the Green Qahlah member, besides growth-sections in the Jafnayn Formation, it is envisaged that faulting took place throughout the development of the Fanja Basin. Therefore, timing of fault-growth encapsulates the Maastrichtian to Late Palaeocene.

In the central part of the outcropping basin, relationships between the Al Batah and Wadi al Theepa members are displayed in a key section longitudinal to the range-front fault (Figure 3d). Beds of the Wadi al Theepa member are folded into a gentle monocline, seen as a change in strike from easterly to south-easterly directions. Farther southeast, Wadi al Theepa member beds can be traced to the Range-front fault where they are truncated. Of significance is the observation that the Al Batah member wedges upwards over the constantly thick units of the Wadi al Theepa member, within the limb of the N-S trending, east-facing gentle monocline. The composite or transitional contact along the base of the Al Batah member is slightly truncating and down-cutting south-westward into Wadi al Theepa member (Figure 3d), locating an unconformity surface. The two members are of comparable thicknesses (Figure 7), but notably, there is a distinct change in facies at the boundary between the Wadi al Theepa and Al Batah members, with significant increase of fine-grained interbedded facies and normal-grading sandstone units in Al Batah member, compared with mainly structureless coarse clastic deposits towards the western end of the basin.

Key in understanding the basin is that the Wadi al Theepa member to the west predates the Al Batah member to the east. The latter succession is overlying a truncation of the Wadi al Theepa member in the monocline, coupled with an eastward thickening of the Al Batah member, signifying Al Batah member growth during folding. The main depocentre for Al Batah member is in the orthogonal syncline oposing the major jog in the Range-front fault.
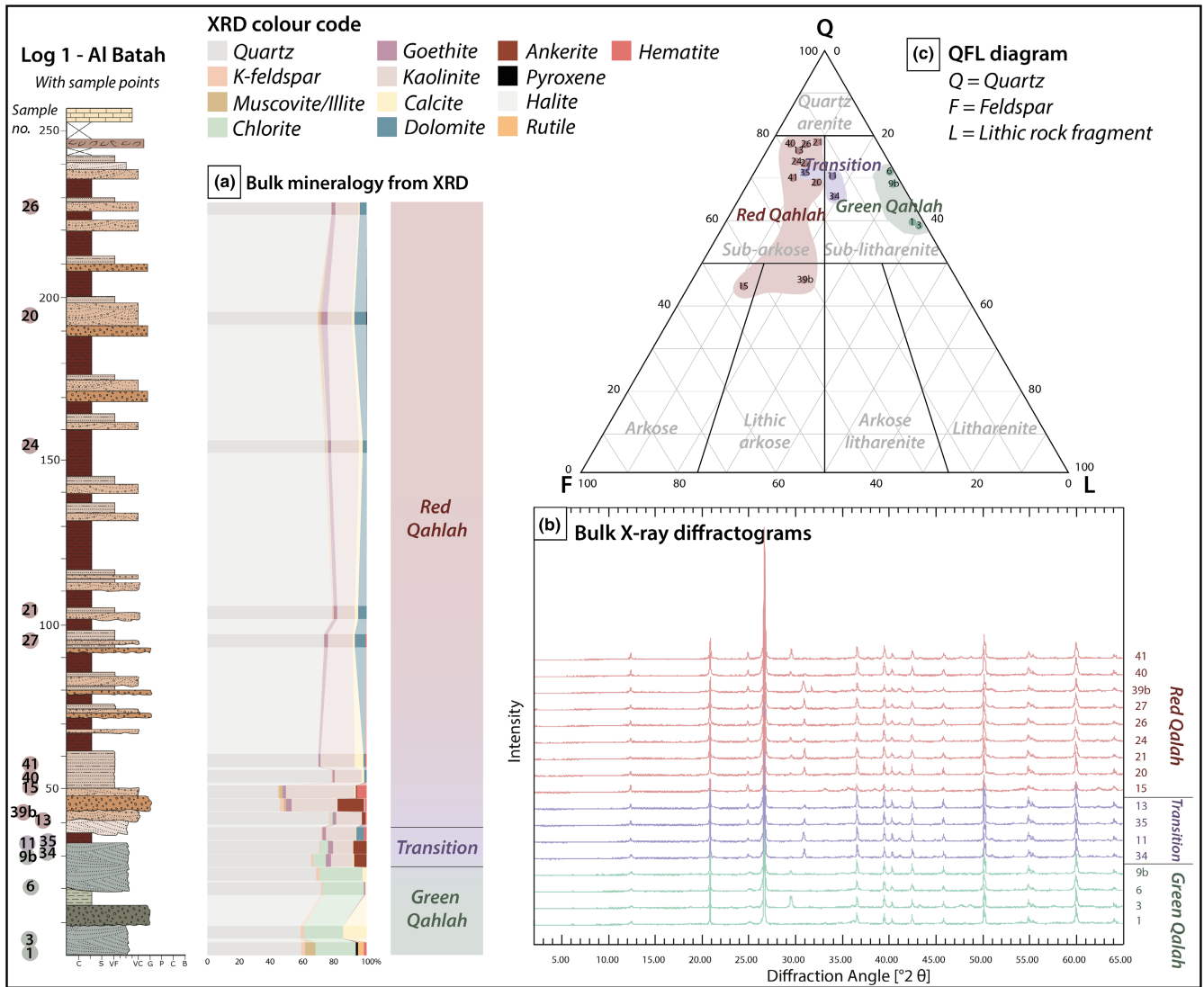
FIGURE 4 Bulk mineralogy from XRD of 17 sandstone samples through the green and red Qahlah members summarised in an average mineral composition plot (a) interpreted from the bulk X-ray diffractogram (b). The sandstones are classified in a QFL diagram (c) where green Qahlah member sandstones plot as sub-litharenites, whereas the red Qahlah members as sub-arkoses to arkosic and lithic arkosic, and the transitional samples plot in the middle between sub-arkose and sub-litharenite. Sample intervals are marked in the key log (Al Batah) on the left-hand side.

4.2 | Sedimentological analysis: Facies and facies associations

Twenty-one facies (named facies A to U) were defined in the Qahlah Formation based on observations of grain size, texture, and sedimentary/biogenic structures, which were used to infer the depositional processes responsible (summarised in Table 1). These facies combine into six major facies associations (FA) that are described and interpreted in detail in the following section and summarised in Table 2. The sedimentological analysis suggests that the Qahlah Formation was deposited in broadly three depositional environments: (i) axial draining braided streams, (ii) transverse draining alluvial fans (inner to

FIGURE 5 Mineralogical characteristics of (a) the green Qahlah member at Al Batah and (b) the red Qahlah (Wadi al Theepa member) at Wadi al Theepa visualised by SEM micrographs with elemental distribution mapping and thin-section images seen through plane polarised light (PPL) and cross-polarised light (XPL). (a) The green Qahlah member (sample 3) shows a clear dominance of silica concentrated in fine sub-rounded mono- and polycrystalline quartz grains (a3,4) with secondary large concentrations of sub-angular lithic rock fragments (a3,4) and cement dominated by calcite and ferric minerals (a1,2). (b) The large proportion of silica in the red Qahlah (Wadi al Theepa member, sample 41) is concentrated primarily in coarse, sub-angular to sub-rounded (radiolarian) chert grains with secondary poly-crystalline quartz grains and partly dissolved kaolinite fragments (b3,4). Cementation is primarily kaolinitic, calcite, magnesium, or ferric (b1,2).

(b) Red Qahlah - sample 41 (Wadi al Theepa, 56 m)
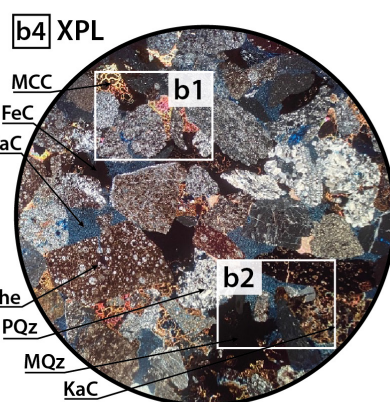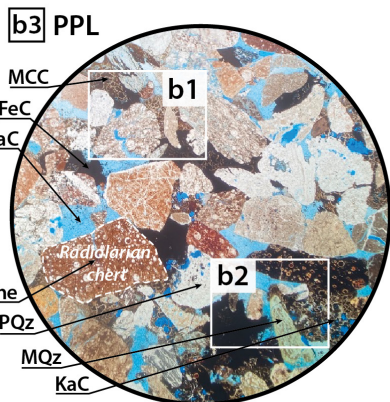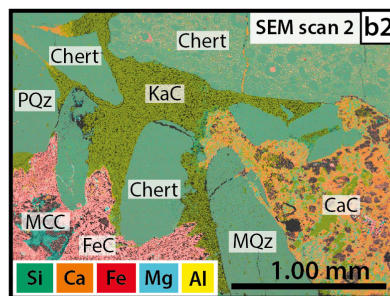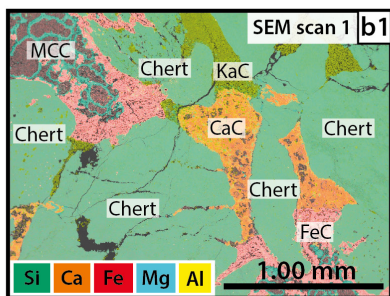
(a) Green Qahlah - sample 3 (Al Batah, 5 m)
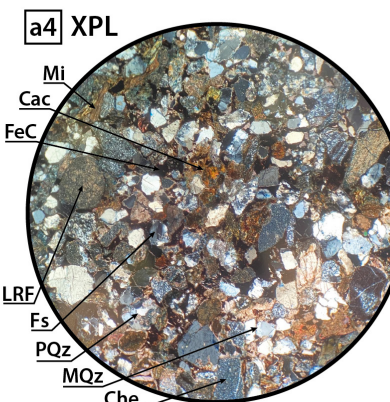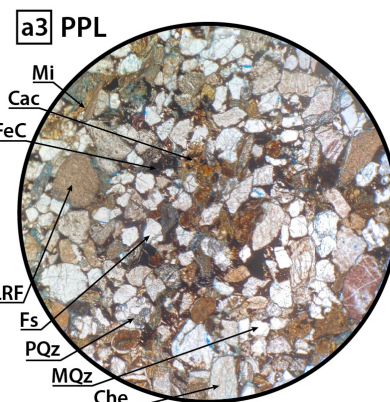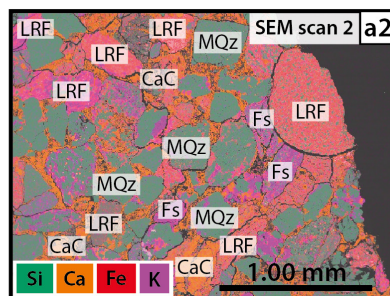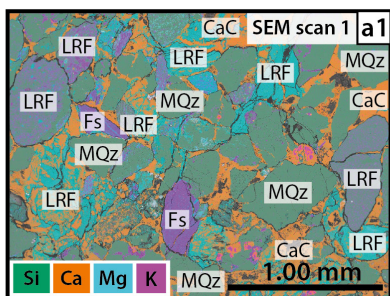
Abbrevations:

CaC = Calcite cement;   **Che** = Chert;   **FeC** = Ferric cement;   **Fs** = Plagioclase/orthoclase;
KaC = Kaolinite cement;   **LRF** = Lithic rock fragment;   **MCC** = Magnesium-Calcite cement;
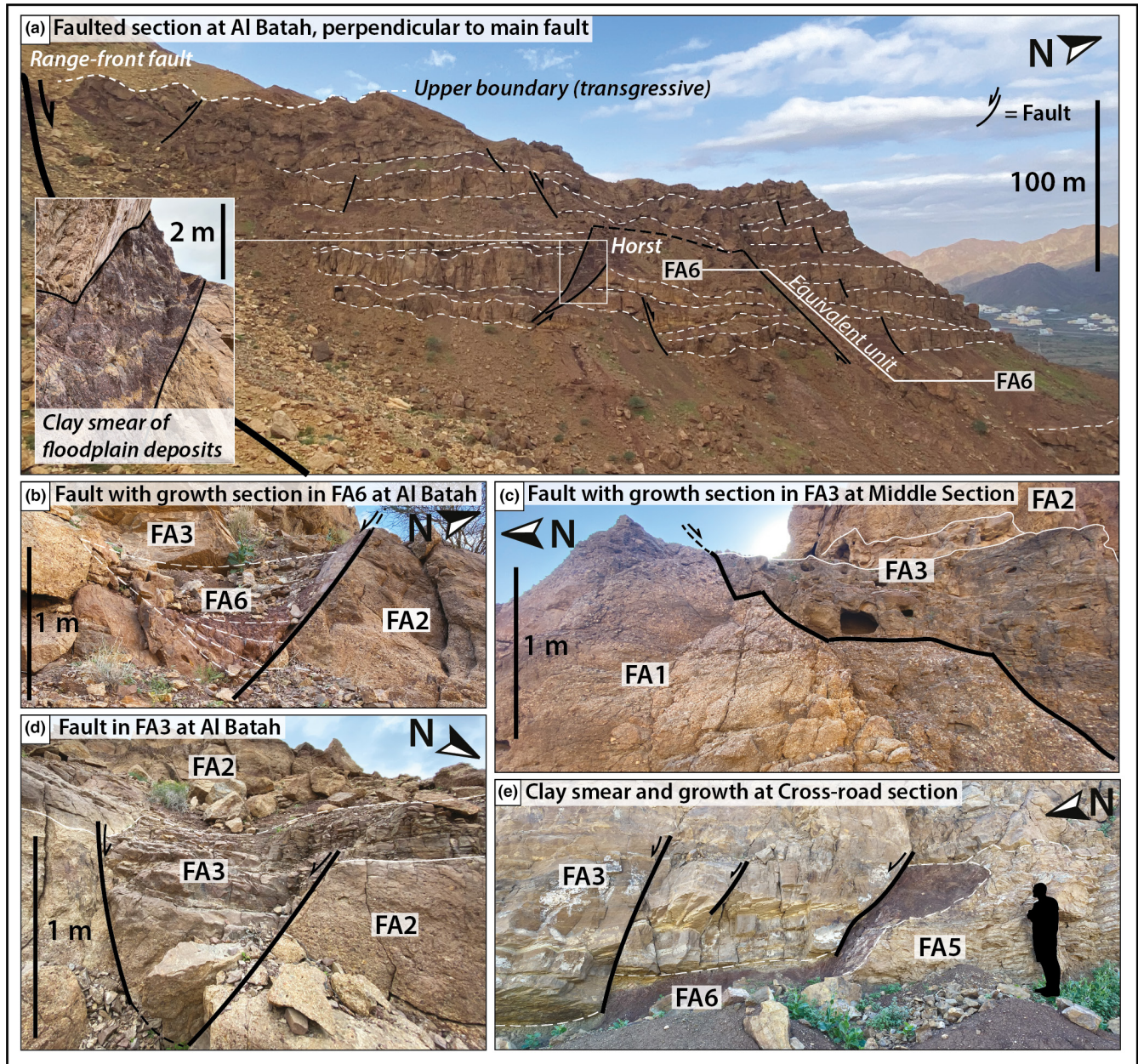**Mi** = Mica;   **MQz** = Mono-quartz;   **PQz** = Polyquartz

FIGURE 6 Representative pictures of faulted sections in the Qahlah formation from 100-m scale (a) to 1-m scale (b–e). (a) S-N cross-sectional view through the Al Batah outcrop displaying intensive internal normal-faulting both synthetic and antithetic. Particularly striking is a 2–3 m thick clay smear (inset photo) in the south-hinge of a horst-structure in the central part of the outcrop. (b–d) Metre-scale faulting in tops of conglomerate beds hosting mini-depocentres filled by finer-grained facies, some exhibiting clear signs of growth (a). (e) Faulting at base of sand-section into underlying fine-grained unit with clay smear. Refer to Figure 3a for locations.

outer zone), and (iii) floodplains with the facies associations defining the elements characteristic to each of these environments. The Green Qahlah member is mainly defined by braided streams (FA4), floodplain and lacustrine environments (FA6) with more rare intermittent small gravity-dominated fault-scarp fans (FA1) (Figure 8b). Deposition in the overlying Wadi al Theepa member was characterised by alluvial fans dominated by gravity- (FA1) and hyperconcentrated flows (FA2) and minor floodplain deposition (FA6), whereas the Al Batah member saw

extensive floodplain deposition (FA6) and fans dominated by hyperconcentrated- (FA2) to stream flows (FA3) and some overbank splay deposition (FA5) (Figure 8c). A high lateral and vertical heterogeneity is characteristic to continental basins (Martinius et al., 2014; Sharp et al., 2003), and these environments may have existed contemporaneously to each other, even if only a succeeding relationship is preserved in the succession. In the Fanja Basin, the outcrop resides in a proximal position to the basin-bounding fault. The distal expression of the system is lacking,

probably due to lesser preservation-potential as accommodation was less in distal areas, and due to more erodible, distal sediment-types (i.e. mudstones and silt) (e.g. Davies et al., 2011; Evans, 1991).

4.2.1 | FA1: Gravel-rich hyperconcentrated flow deposits

4.2.1.1 | *Description*

The conglomerate-dominated facies association 1 (FA1) occurs in metre-thick units consisting of 20–150 cm-thick coalesced interbeds of predominantly facies A and B and D, with subordinate Facies C (Table 1; Figure 9a). Transitions between the interbeds are diffuse and FA1 may appear structureless with lateral and vertical grading. Internally, interbeds are most commonly tens of cm in thickness and tens of cm to a few metres in lateral extent. The beds may occur isolated within finer grained facies (e.g. FA6) with sharp lower contacts and sharp to transitional upper boundaries, or, more commonly, interstratified with FA2 with diffuse transitions between the two, defined by variations in clast concentration (Figure 9b–e). Where FA1 occurs in combination with FA2 and FA3, FA1 appears as thin, in places repetitive, more clast-rich, poorly sorted, disorganised intervals. Where distinguishable in association with FA2, FA1 beds have a tabular to irregular geometry with laterally cuneate shapes in places, commonly exhibiting a stacked layer-cake stratigraphy. Together, FA1, FA2 and FA3 may form thick, laterally extensive units (Figure 9). There is a wide variability in sediment transport direction between western and eastern outcrops but with an overall northward transport direction (Figure 10b).

4.2.1.2 | *Interpretation*

The gravity to hyperconcentrated flow regime processes responsible for deposition of FA1 (Table 1) is in combination characteristic to high slope areas in the inner to medial zone of alluvial fans (Table 2; Blair, 1999a; Gao et al., 2020; Miall, 2010; Sohn et al., 1999). The immaturity of the sediment is expected due to the proximity to the source in the footwall and the rapid depositional processes with discontinuous flows giving rise to minor wash-out and a low sorting degree (Blair, 1999c).

4.2.2 | FA2: Mixed gravel- to sand-rich stream flow deposits

4.2.2.1 | *Description*

The mixed conglomerate- to sandstone-dominated facies association 2 (FA2) occurs in up to 25 m-thick units with lateral extent up to hundreds of metres. Internally, FA2 consists predominantly of closely interstratified facies B and C and minor facies A and D (Table 1; Figure 9a,c). Interbed boundaries lack sharp contacts and appear as transitional changes in clast abundance and colour (Figure 9c). FA2 most commonly occur as amalgamated units interbedded with thick red mudstone intervals of facies association 6 (Figures 3d and 9a). Lower boundaries to FA6 are distinctly sharp and erosive, whereas upper boundaries may be transitional into FA6. Some upper contacts are faulted forming small (a few metres scale) depocentres form in the tops of the conglomeratic beds, filled by FA6, with evidence of growth (Figure 6b). Similar palaeodrainage directions as FA1 are recorded in FA2 with a northward dominance (Figure 9b).
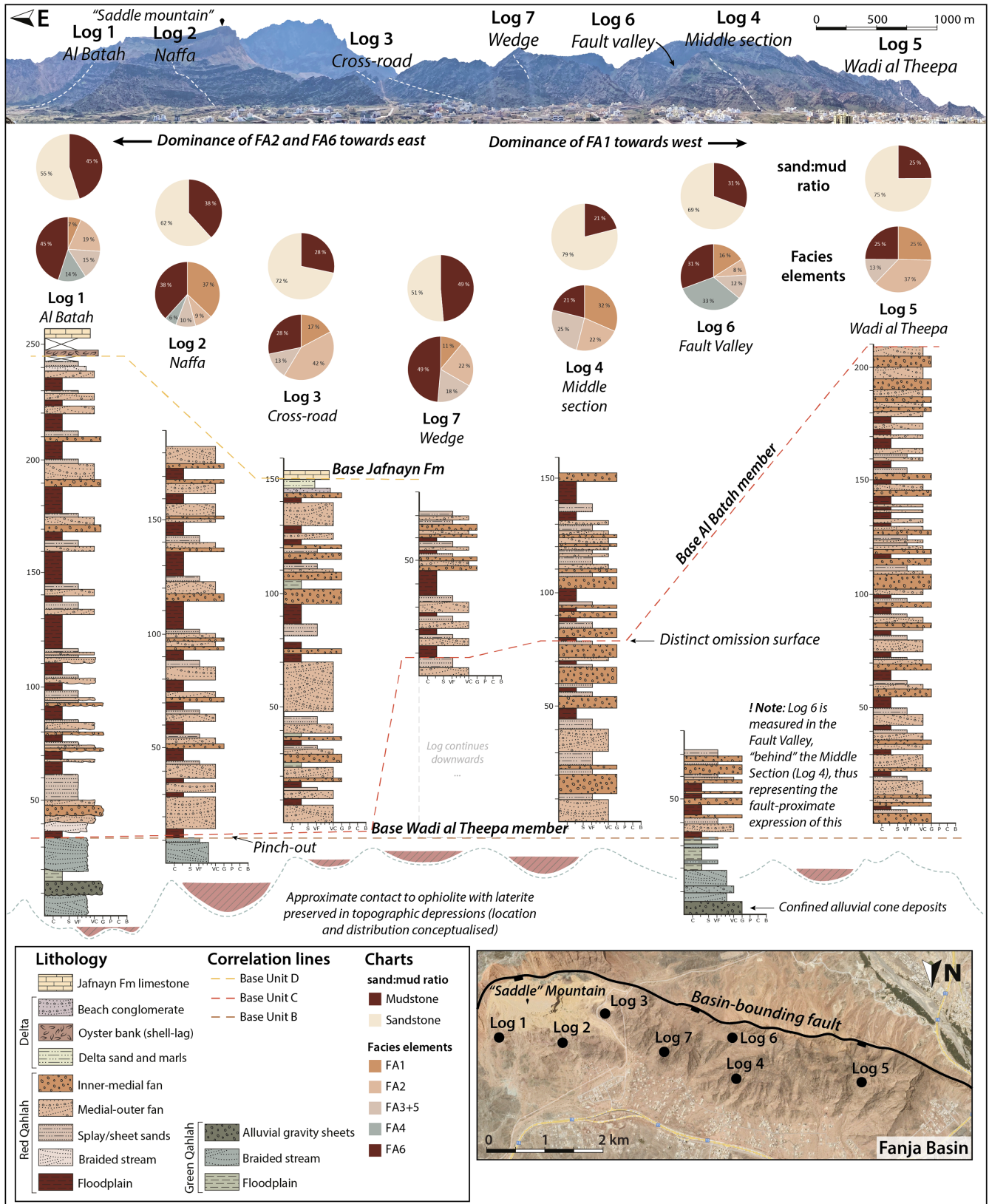
4.2.2.2 | *Interpretation*

The prevalence of stream-flow generated structures (Facies C; Table 1.1) over gravity-driven ones along with better sorting compared with FA1 suggests deposition in an area of shallower slope on alluvial fans (Evans, 1991; Jo et al., 1997; Miall, 2010). However, being dominated by Facies B (Table 1.1), FA2 is positioned in the transitional regime between turbulent flow and traction-flow (Sohn et al., 1999). The combination is by some termed 'hyperconcentrated flows', which are common in the medial fan-zone where the fan slope decreases significantly and the streams of the active fan lobe splits into smaller, shallower streams (Table 2; Gao et al., 2020; Siegenthaler & Huggenberger, 1993; Sohn et al., 1999). Much of the sedimentation here takes place through flashy, widespread, sheet-like deposition (Blair, 2000). The facies D likely result from scour pool fills, which are common features in alluvial fan surfaces (Gao et al., 2020).

4.2.3 | FA3: Sand-rich flash flood and minor stream deposits

4.2.3.1 | *Description*

The sandstone-dominated facies association 3 (FA3) occurs in up to 5 m-thick, thinly-bedded units with a sheet-like geometries (Figure 11d–f). Facies E, F, G, H, I, and less commonly Facies B and C, represent the main constituents in FA3 (Tables 1.1 and 1.2). FA3 occurs in close association with FA1 and FA2, interbedded between these, commonly in stratigraphic or structural lows (depocentres) of these (Figure 6b–e), with transitional boundaries except when fault-bounded. The occurrence of FA3 may also mark a grading transition from FA1 and/or FA2 into FA6. Furthermore, a trend is observed where FA3 occurs interbedded with FA5 with either sharp or transitional contacts between these (Figure 11d).

4.2.3.2 | Interpretation

FA3 was deposited by flash floods and minor streams primarily in the outer fan zone (Table 2; Gao et al., 2020), according to the sheet-like geometries, rapid depositional features (i.e. soft sediment deformation; Burns et al., 2017), and the higher proportion of sand relative to clasts compared with FA1 and FA2, but in close relation to these two facies associations. These types of deposits are common

FIGURE 7 Sedimentary logs in E-W panel with correlation of major stratigraphic surfaces flattened at the base Wadi al Theepa member. Lithologies in the logs are conceptualised to represent the dominant facies associations through the logged intervals with the facies associations proportions and sand:mud ratio at each logged location summarised in pie-charts above the logs. Overall these shows an increase of fine-grained deposits (FA6) and hyperconcentrated- to stream-flow-generated coarse clastics (FA2) in the eastern Fanja Basin, whereas gravity-flow-generated deposits (FA1) dominate the western Fanja Basin with only minor fine-grained interbeds. The lower boundary to the ophiolite is not exposed in the basin but the approximate contact is visualised to illustrate the topographic relief expected in the surface, with laterite preserved in topographic lows. The positions of logs are shown both in a E-W outcrop photomosaic (top) and in satellite basin view (bottom). Note that log 6 was logged in the Fault Valley, which is perpendicularly positioned south of the middle section log 4 in a more fault-proximal position to this and thus does not represent a basin-axial thickness-profile, but rather a basin transverse thickness-profile.

to upper-flow-regime flash floods and reworking of these during overland flows through longer periods between floods (Blair, 2000). Another common constituent of the dried-out fan surface during inactivity is aeolian deposition (Facies H; Table 1.1), where dunes develop in the topographic lows of the rugged fan surface (Blair, 2000; Leleu & Hartley, 2018).

4.2.4 | FA4: Sand-rich braided stream deposits

4.2.4.1 | Description

Facies association 4 (FA4) dominates the lower part of the Qahlah Formation in the Fanja Basin (Green Qahlah member) and is composed of tens of cm to few metres thick beds of dominanted by the sandy facies' J, K and L (Table 1.2), and secondarily facies' A and F (Table 1.1), interbedded in 1–20 m thick units. Beds are amalgamated with rare occurrences of fine-grained deposits (FA6) in between (Figure 12c). Laterally, reactivation surfaces and erosive contacts divide internal beds and bedsets. When Facies A is present within FA4, it is localised (Figure 3a; Figure 12a) and has sharp to erosive contacts to surrounding facies. The sedimentary transport direction is west-northwest in the units dominated by facies J, K and L, whereas azimuths in beds of Facies A trend north-northeast (Figure 10a).

4.2.4.2 | Interpretation

The grain size spectrum (medium- to coarse-grained sandstone, gravel and conglomerate), sedimentary structures (e.g. trough cross-bedding and downstream accretion bars), multi-storey stacking with no preserved overbank deposits, lack of lateral accretion elements, and incomplete upward fining channel profiles in FA4 in combination suggests that these are deposits of high-discharge braided streams (Table 2; Ashmore, 1985; Hjellbakk, 1997; Jones et al., 2001; Miall, 1997a, 1997b; Nichols & Fisher, 2007). The presence of Facies A may result from activation along the Range-front fault and the rapid input of coarse clastics consequently hereof, inferred by the predominant

direction of sedimentation perpendicular to the Range-front fault in a unit elsewise characterised by parallel-to-fault drainage.

4.2.5 | FA5: Heterolithic overbank deposits

4.2.5.1 | Description

Facies association 5 (FA5) occurs locally in 1–5 m thick units of repeated thin bedded sandstone and silt (Facies N; Table 1.2) stacked in coarsening and thickening upwards units Figure 11a–d. The facies either occur as repetitively stacked heterolithic beds of Facies N, or the more structureless, slumping Facies M, and is commonly observed in association with FA5 and FA3 or FA2, with sharp, in places erosive, boundaries to these.
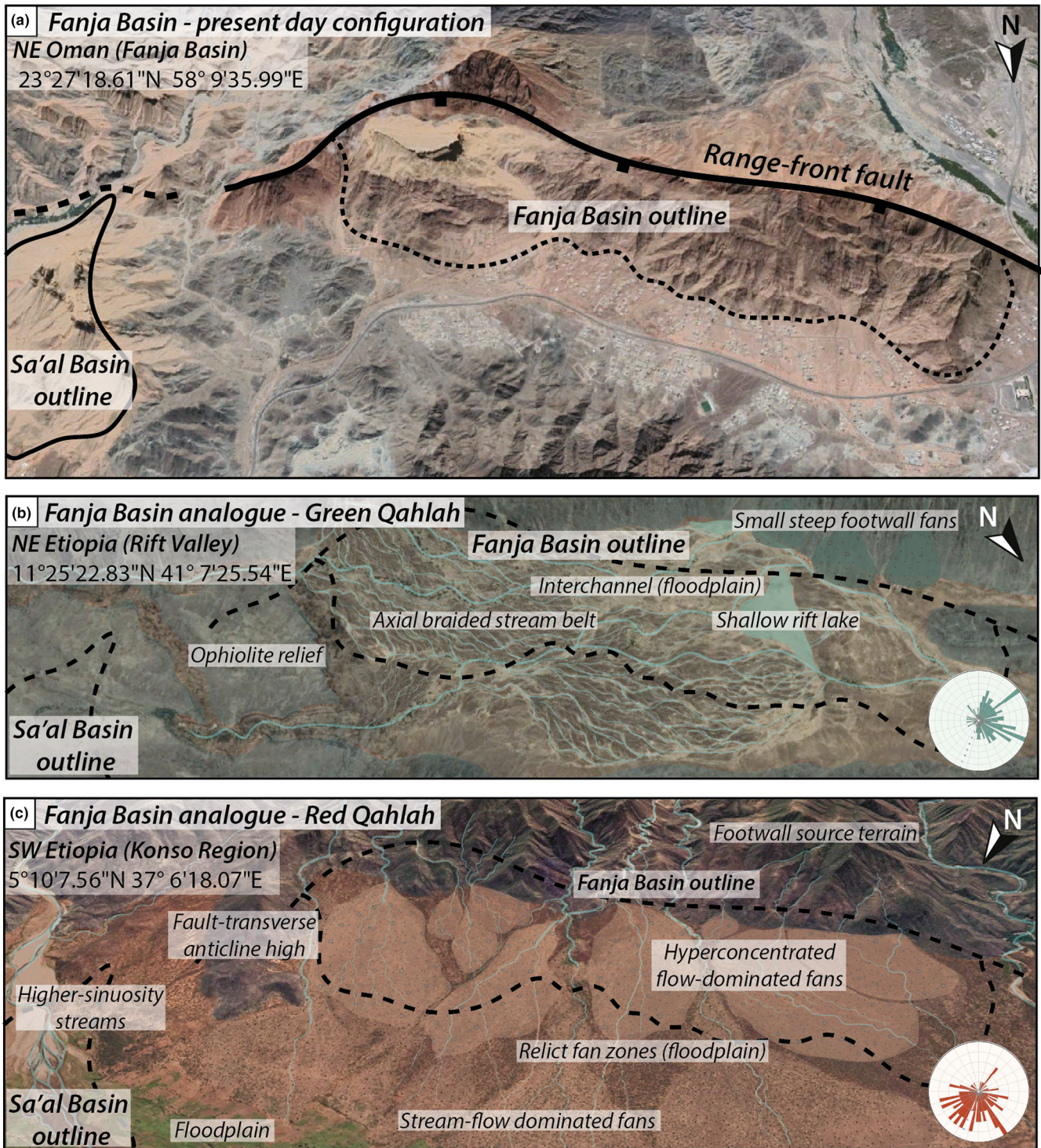
4.2.5.2 | Interpretation

FA5 may represent crevasse- and overspill splay sands deposited onto wet substrates such as the floodplain or into standing bodies of water (Table 2). This interpretation reflects the thinly bedded architecture, inversely-graded- and upwards-thickening-trend, and sedimentary structures representative to the facies combination in FA5 (Table 1.2). These are all factors common to prograding depositional elements, such as crevasse splays (Facies M; van Toorenenburg et al., 2018) and small lacustrine deltas (Facies N) (Burns et al., 2017; Gulliford et al., 2017).

4.2.6 | FA6: Fine-grained floodplain deposits

4.2.6.1 | Description

Facies association 6 (FA6) occurs either in thick laterally extensive units between coarser-grained fan (FA1, 2, 3) or fluvial (FA4) strata, or as intermittent thin "pockets" between these with a marked lateral pinchout (Figure 13a). FA6 varies in character between structureless red mudstone to grey-red silt with very fine to fine-grained sand interbeds (Figure 13d). FA6 may have a graded profile from fine-grained planar

(a) Fanja Basin - present day configuration
NE Oman (Fanja Basin)
23°27'18.61"N 58° 9'35.99"E

Range-front fault
Fanja Basin outline
Sa'al Basin outline

(b) Fanja Basin analogue - Green Qahlah
NE Etiopia (Rift Valley)
11°25'22.83"N 41° 7'25.54"E

Small steep footwall fans
Fanja Basin outline
Interchannel (floodplain)
Axial braided stream belt
Shallow rift lake
Ophiolite relief
Sa'al Basin outline

(c) Fanja Basin analogue - Red Qahlah
SW Etiopia (Konso Region)
5°10'7.56"N 37° 6'18.07"E

Footwall source terrain
Fanja Basin outline
Fault-transverse anticline high
Hyperconcentrated flow-dominated fans
Higher-sinuosity streams
Relict fan zones (floodplain)
Sa'al Basin outline
Floodplain
Stream-flow dominated fans

bedded sandstone (Facies O) over rippled silt (Facies P) into red mudstone (Facies Q), commonly containing abundant rhizoliths and occasional yellow-white horizons (Table 1.3; Figure 13). Lower contacts may be transitional from FA2 or FA3 into FA6, or sharp when filling in a faulted depression in the coarser units (Figure 6b,c), or forming sharp surfaces (e.g. at 78 m in Log 4). Upper contacts to coarser facies are erosive and sharp (Figure 13a–e). Lateritic soils are also included

in FA6 but these occur only locally at the base of the succession and are poorly exposed.

4.2.6.2 | Interpretation

FA6 are deposits of wet, vegetated floodplains with minor flow-activity (Table 2). This conclusion is based on the presence of continental depositional indicators within the mudstone-dominated intervals (e.g. rhizoliths) and the intimate association with alluvial deposits

FIGURE 8 (a) Satellite photo of the present-day Fanja region with the Fanja Basin and Sa'al basin outlined in black. (b) Satellite photo of a narrow continental rift valley in NE Etiopia (part of the east African rift), which represents a suitable present-day analogue to the Fanja Basin during deposition of the green Qahlah member. The system exhibits similar basin geometry, scale, drainage and sedimentary processes, where a westward draining braided stream system dominates with small, steep fans along the faulted basin-margin. Main depositional elements representative to the Fanja Basin and present in this modern system is labelled. The Fanja Basin outline is projected onto the photo, and main depositional elements are highlighted with labels showing the analogue elements, as they would have occurred in the Fanja Basin during deposition of the green Qahlah member. (c) Satellite photo of a mature continental rift valley in SW Etiopia (Konso region), which represents a suitable present-day analogue to the Fanja Basin during deposition of the red Qahlah members. The outline of the Fanja and Sa'al basins is projected onto the photo. Similarly to the Fanja Basin, a fault-transverse anticline high to the east divides two basins. The basin west of this anticline is, like the Fanja Basin, dominated by northward outbuilding alluvial fans fed through fault-transverse sediment inlets, whereas the basin east of the anticline high is dominated by floodplain deposition and higher-sinuosity streams, similar to what is observed in the Sa'al basin stratigraphy. Main depositional elements representative to the Fanja Basin and present in this modern system is labelled. The collected PC measurements for the members are presented in rose diagrams to the lower right of the figures.

(FA1-3). Root-traces indicate soil-forming processes operating during deposition (Schieber, 1999; Zhang et al., 2021). The presence of silt and sand lenses within FA6 indicate erosional bedload transport or minor spill deposits from nearby channels, but the dominating structureless mudstone facies (Q) suggests that flow velocities rarely exceeded the threshold of motion for silt and sand (Schieber, 1999). The fining-upwards is consistent with a gradual abandonment where flow-processes decrease, coarse sediment input ends, and deposition shifts to suspension (Ghosh et al., 2006), likely related to the common shifting position of alluvial fan lobes (Blair & McPherson, 2009). The red colouration reflect haematite pigmentation (Eren et al., 2015), which is often associated with continental environments as process requires oxidising conditions.

4.3 | Boundaries

Boundaries or transitional sections between homogenous units commonly represent changes in the basin configuration (e.g. Steel, 1993). In the Fanja Basin, the lower unconformable boundary to the ophiolite is not exposed, but studies of equivalent successions in other basins around the Al Hajar Mountains show an irregular unconformative contact (e.g. Abbasi et al., 2014; Alsharhan & Nasir, 1996; Nolan et al., 1990), which is sharp except when overlain by laterite. The overlying Green Qahlah member has a sharp and erosive contact to the underlying laterite (Figure 14a,b).

In the east, the boundary between Green- to Red Qahlah is marked as a gradual transition in colour over 2–7 m through sandy braided stream facies (FA4; Figure 14c) capped by a sharp contact to the orange-red alluvial conglomerates characteristic of the Red Qahlah members (Figure 14d). This boundary, exposed at Al Batah, marks the eastern pinch-out (Figure 7) of the Wadi al Theepa member (gradual colour change), which

otherwise dominates the western basin, and the base of the Al Batah member (sharp contact). In the western part of the basin, the boundary between the two members of the Red Qahlah discloses a prominent barren surface on top of conglomeratic units of the Wadi al Theepa member, marking a low-angle truncation of these (Figure 14e). Similar surfaces divide conglomeratic bodies (FA1 and FA2) and fine-grained intervals (FA6) throughout the Red Qahlah units, with common duricrust formation in conglomerate tops (Facies R, Table 1.3). The presence of rhizoliths, duricrusts, and palaeosol horizons related to these surfaces all conform to these being (continental) omission surfaces, as described by Kraus (1999) and Del Papa et al. (2010). Duricrusts reflect hardpan formation, indicative of long-exposure surfaces of non-deposition, and are thus important indicators for prevailing climatic conditions and fluctuations in accommodation- and sedimentation rate (e.g. Martinius et al., 2014). This conforms to omission surfaces representing minor breaks in sedimentation without any significant erosion (Bromley, 1975). Overlying beds of the Al Batah member are concordant to the contact, but on 100-m scale can be seen to thin westwards up along the limb of the mentioned N-S trending, east-facing monocline situated in this area.

There is an angular unconformity between the Qahlah and Jafnayn formations, seen as nearly flat beds above the longitudinal syncline of the underlying basin. The boundary is only present in the eastern end of the Fanja Basin and either occur as a sharp contact to beach conglomerates or an oyster lag (Figure 14f,g). Fault contacts on the north and south side of the Jafnayn Formation outlines a graben superimposed on the synclinal Qahlah basin.

4.4 | Vertical and lateral variations

The prominent lateral changes in outcrop geometry (5.1; Figure 3d) are accompanied by notable variations in
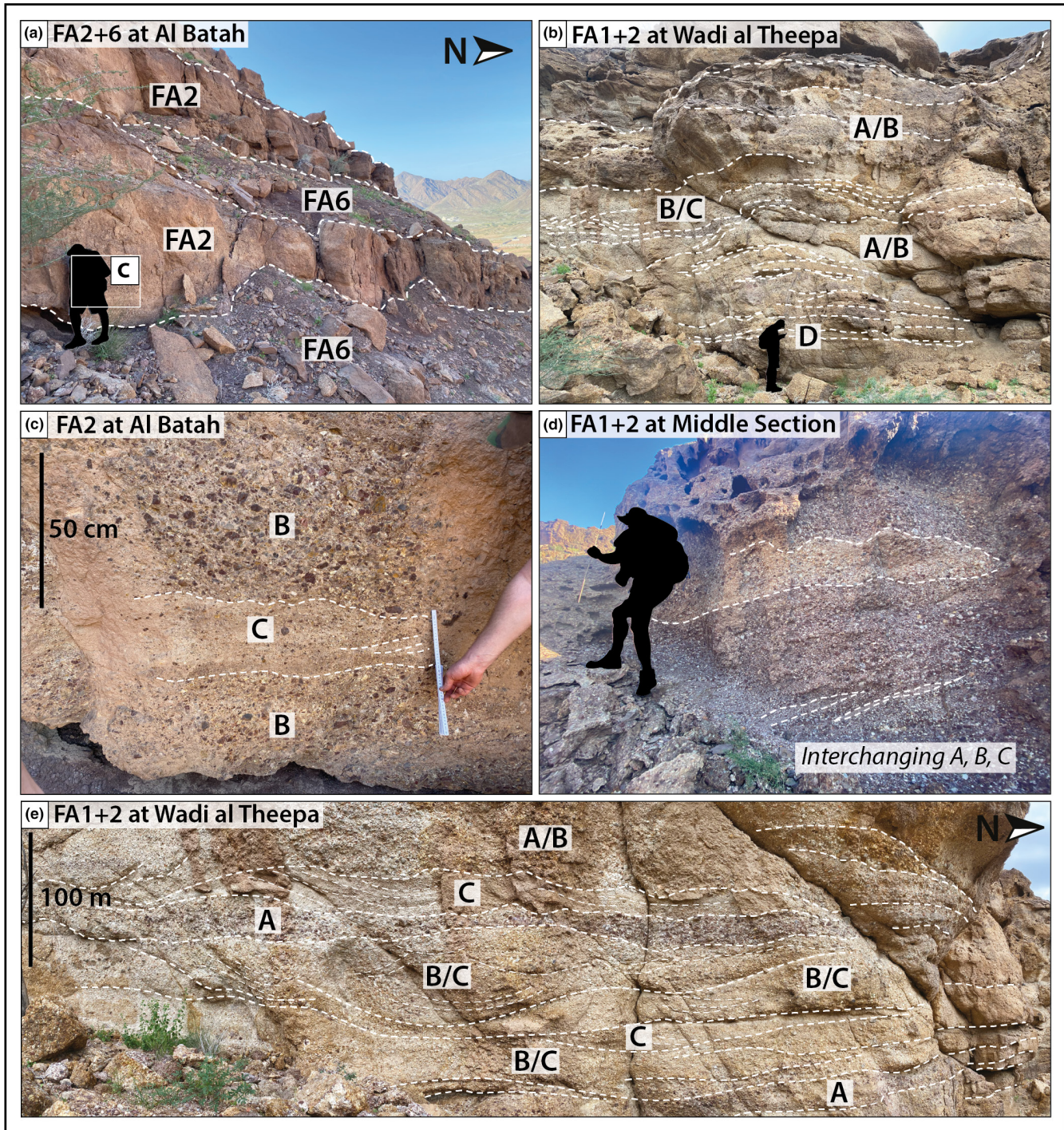
FIGURE 9 Representative photos of FA1 and FA2. (a) Cyclic interbedded tabular FA2 and thick FA6 at Al Batah. (b) Closely stacked, amalgamated beds of facies A, B, C, D (FA1-2) at Wadi al Theepa. (c) Details of FA2 from (a). (d) Facies A, B, and C (FA1-2) interchanging through grain size changes and clast colour variations (middle section). (e) Detail of (b) showing the spatial variation between facies A, B and C. Refer to Figure 3a for locations.

thicknesses and facies distribution within the units, as summarised in Figure 7.

The Green Qahlah member is highly variable from <2 m to 35 m, with parts of the basin (central and distal/north) lacking this unit. Besides well-exposed mountainsides, sandy intervals appear as patchy outcrops in mounts scattered across the valley floor, indicative of dominating fine-grained floodplain facies (eroded) with scattered sandstone channels (preserved). From east, the thickness decreases towards the central part where the Green Qahlah member disappears but reappears furthest to the west in mounts of 1–5 m in thickness.
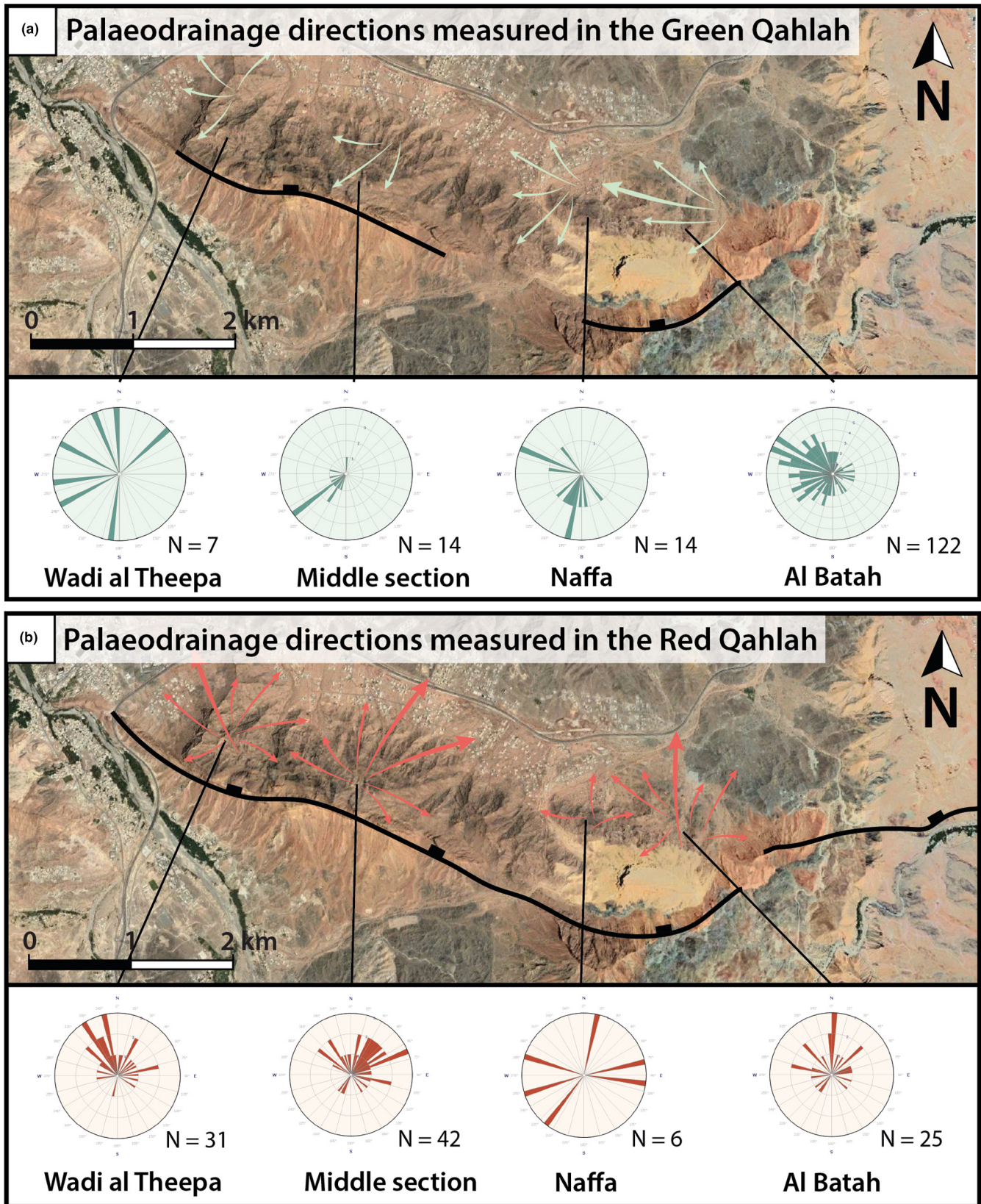
FIGURE 10 Summary of palaeodrainage directions at Al Batah, Naffa, middle section and Wadi al Theepa for (a) the green Qahlah member ($N = 157$) and (b) the red Qahlah members ($N = 104$). Directions are summarised in rose-diagrams for each location. Overall, the green Qahlah member (a) drained averagely WNW, fault-parallel. The red Qahlah members (b) drained averagely northward, fault-transverse, with a larger spread. The Al Batah member (Al Batah and Naffa locations) drainage trended more NNE, whereas the Wadi al Theepa member (middle section and Wadi al Theepa locations) drainage shows a larger spread NNE-NNW.
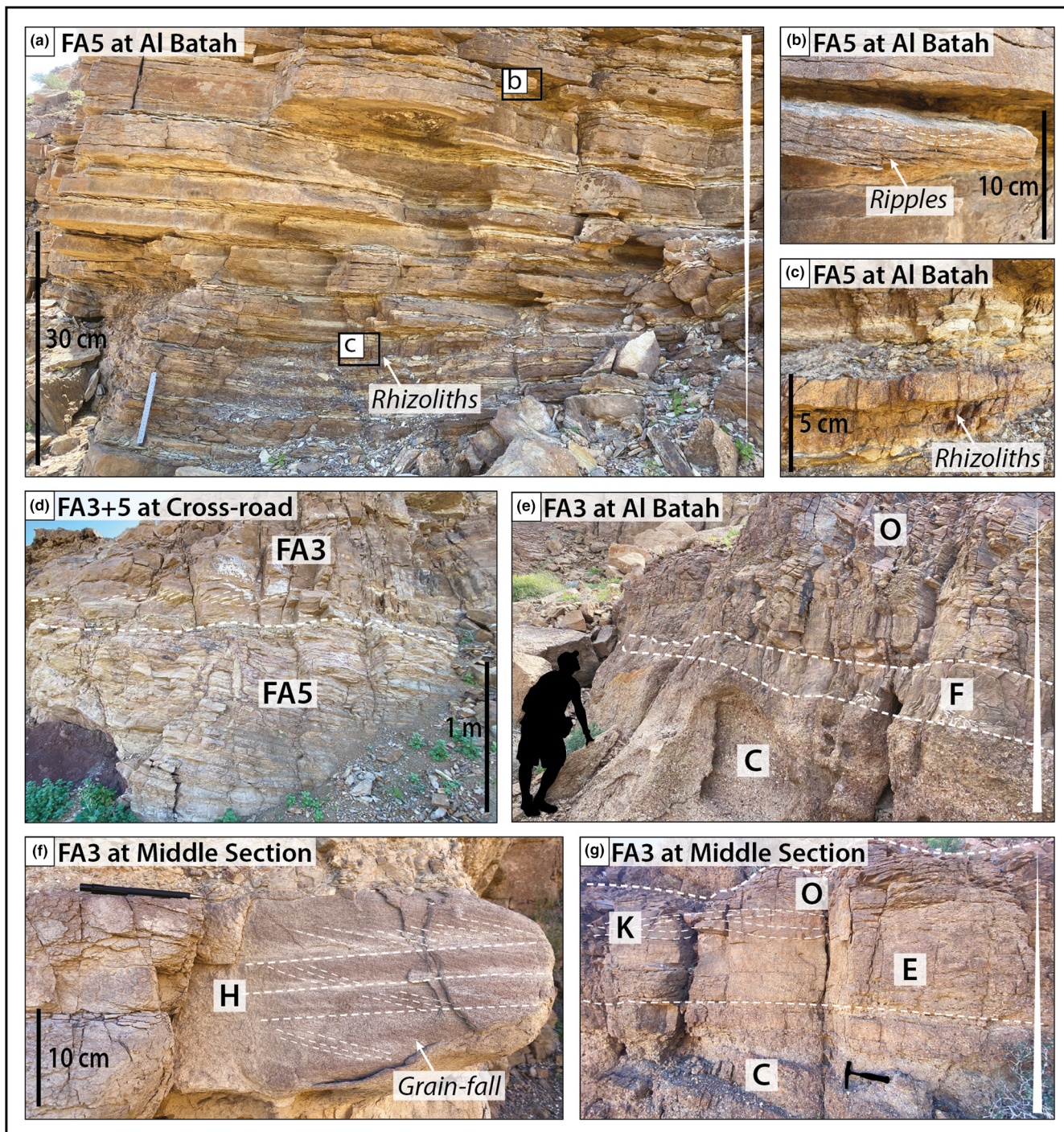
FIGURE 11 Representative photos of FA3 and FA5. (a) Thinly bedded heterolithic upwards coarsening FA5 unit at Al Batah. (b) Detail of (a) showing unidirectional ripples in fine-grained sandstone. (c) Detail of (a) showing dark red rhizoliths through fine-grained sandstone. (d) FA5 transitioning upwards into FA3 at cross-road section. (e) FA3 with soft sediment deformation in fine- to medium grained sandstone (facies F) sharply overlaying FA2 conglomerate at Al Batah. (f) Sets of tangential cross-stratified very fine-grained sandstone (facies H) with sharp contacts to surrounding conglomerate beds of FA1 at middle section. (g) FA2 sharply overlain by a fining upwards FA3 (from facies E into facies O) at middle section. Refer to Figure 3a for locations.

The thickest measured units are in the eastern basin (Al Batah) and in the Fault Valley, closest to the Range-front fault (Figure 7). Furthermore, the Fault Valley section deviates from the commonly braided stream sandstone facies, characteristic for the Green Qahlah member, by hosting large quantities of thick green floodplain mudstone intervals (FA6) and interbedded coarse gravity-driven conglomerates (FA1) (Figures 7 and 12e).
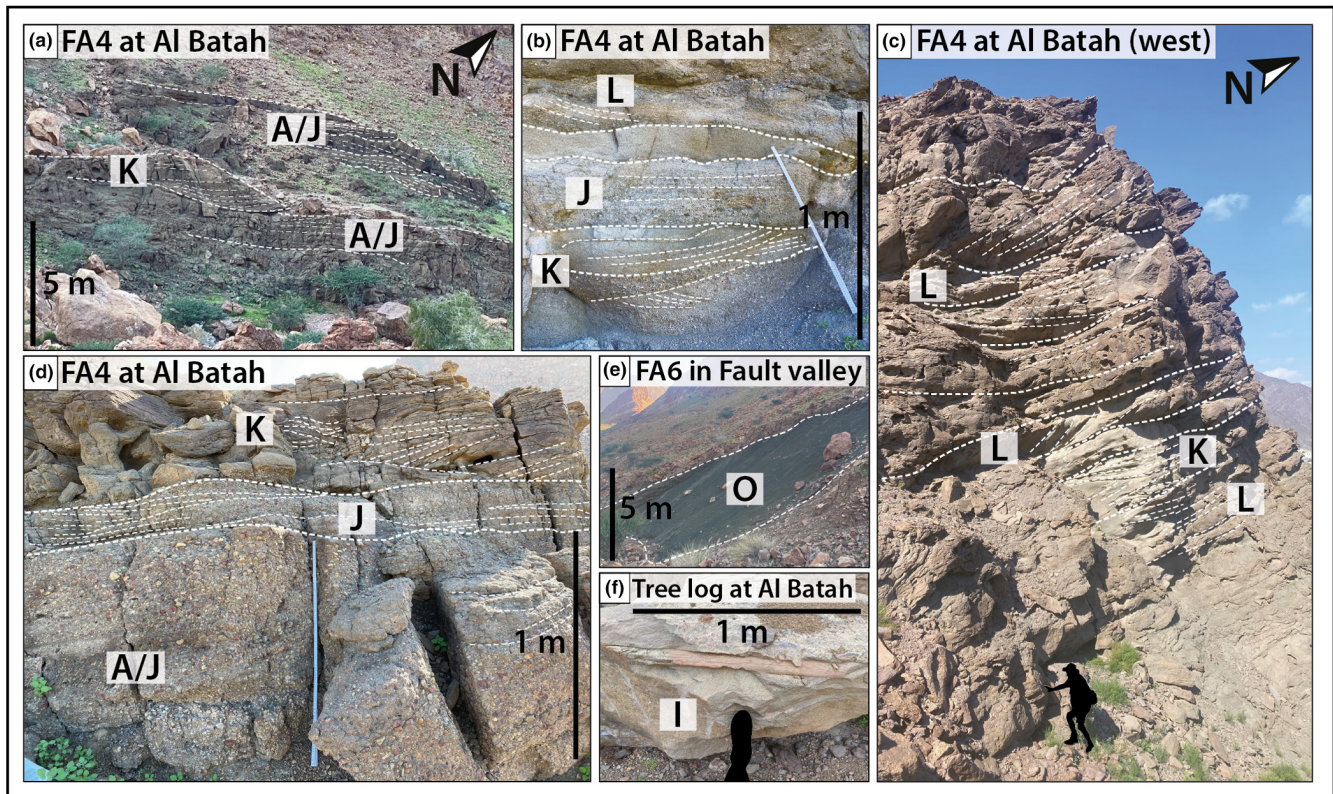
FIGURE 12 Representative photos of FA4 from the green Qahlah member. (a) Gravelly traction carpet deposits with transport northward at Al Batah. (b) Inter-channel dunes (K) and channel-bar (L) deposits of braided streams at Al Batah. (c) Amalgamated unit of composite bars and dunes (facies K,L) of braided streams at Al Batah. (d) Gravity flow to traction carpet deposits (a) sharply overlain by gravelly bar deposits (facies J) fining upwards into inter-channel dune (facies K) deposits at Al Batah. (e) Green floodplain fines (FA6) interbedded with conglomerates of the green Qahlah member in the Fault Valley. (f) Tree log in homogenous massive sandstone (facies I) at Al Batah.

The *Wadi al Theepa member* of the Red Qahlah is characterised by a dominance of coarse-grained deposits (>75%) relative to fine-grained deposits (<25%), whereas the *Al Batah member* exhibits a much higher concentration of fine-grained deposits (28%–49%) relative to coarse-grained deposits (51%–72%) (Figure 7). The Wadi al Theepa member is thickest (210 m) furthest west in the basin at Wadi al Theepa and thins gently eastward before it pinches out between the Green Qahlah and Al Batah members into the eastern depocentre. The Wadi al Theepa member is dominated by stacked beds of interbedded FA1 (25%) and FA2 (37%) between thinner intervals of FA6 (25%) with minor FA3 and FA5 (13%) (Figure 7). The Al Batah member is concentrated in the eastern basin with the thickest succession measured at Al Batah (243 m) and thins westward pinching out in the western part on top of Wadi al Theepa member. At the thickest point, the unit is dominated by FA6 (45%) interbedded with stacked beds of FA2 (19%) and FA3 and FA5 (15%) with minor FA1 (7%) (Figure 7).

In summary, the Fanja Basin is overall made up of a basal succession of green braided stream deposits (Green Qahlah member), concentrated in the east and towards the central fault segment. Noticably, thicker sections of the Green Qahlah locates in two areas where the Range-front fault offers former relays, a common entry point for sediments into hanging wall basins (e.g. Gawthorpe & Leeder, 2000). The overlying Wadi al Theepa member contains a coarse-sediment dominated succession with secondary fine-grained intervals concentrated in the western basin. A fine-sediment dominated succession with secondary coarse-grained intervals in between, the Al Batah member, concentrates in the eastern basin. Finally, the succession is capped in the eastern basin by a transgressive surface followed by deltaic sandstone and marl deposits, and topped by a thick limestone succession (Figure 7).

4.5 | Palaeodrainage directions

Palaeocurrent (PC) trends provide important information on the overall trend of drainage through a basin, where the entry points for drainage into the basin was, and furthermore indicate the dominant facies
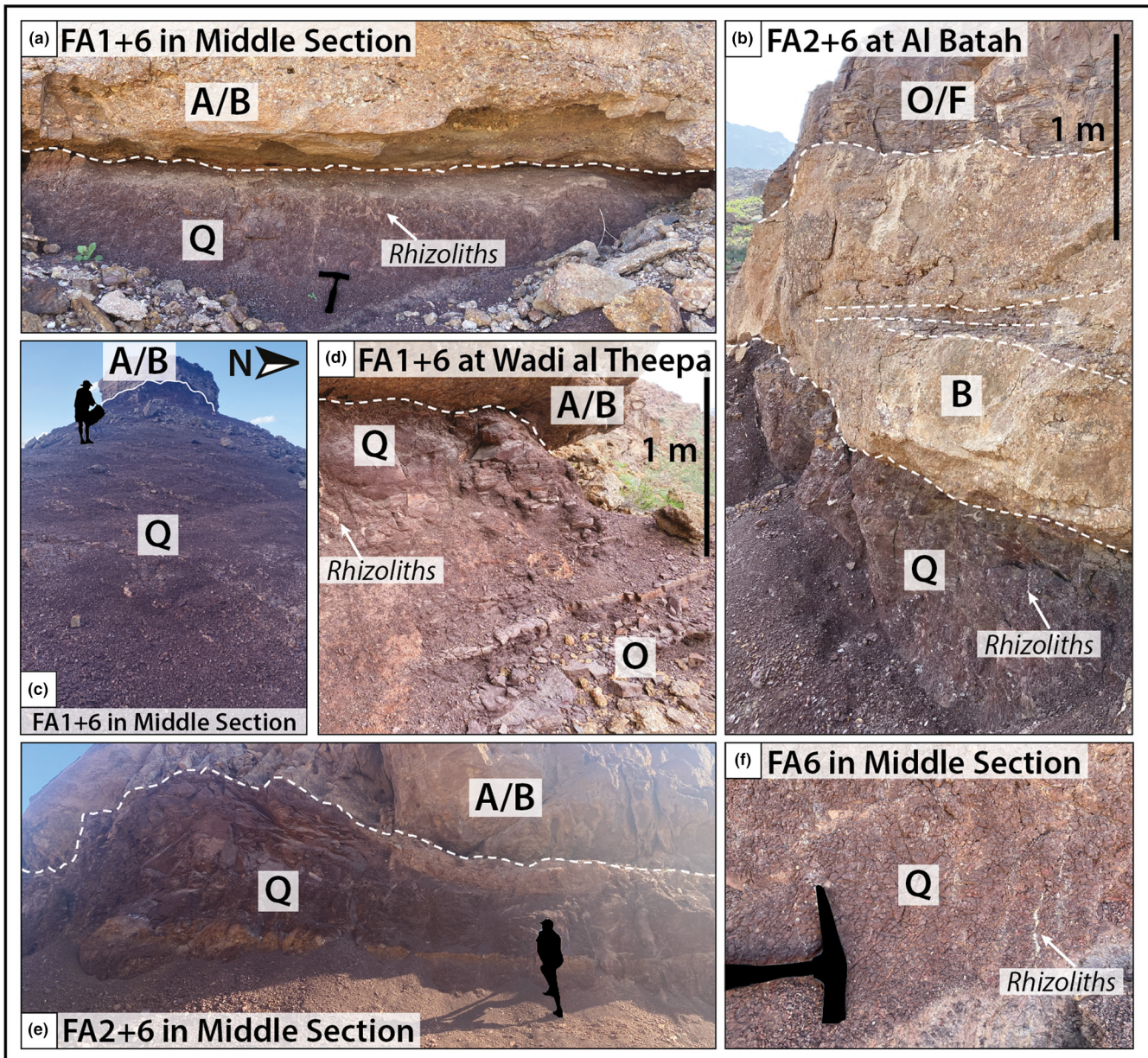
FIGURE 13 Representative photos of FA6 showing sharp contacts to overlaying conglomerate beds of FA1 /2 (a–e), and internal features such as rhizoliths (a,d,f), subtle variations between clay and silt fractions (d), and mottling due to kaolinisation or pedogenic processes. Refer to Figure 3a for locations.

type according to the spreading of the measurements (Tucker, 2003). Figure 10 summarises the PC data collected for this study.

The Green Qahlah member shows an average eastward PC trend along and slightly towards the Range-front fault with dominant directions WNW to WSW (Figure 10a). In the eastern part (Al Batah), there is a clear dominance of east to ENE trending azimuths. In the central basin (Naffa and Middle section), the PC's trend more southeast, whereas a wider spreading from south to northwest dominates the western basin (Wadi al Theepa) (Figure 10a). In accordance with the

facies analysis, the along-fault PC trend with a crescent spreading is typical for (braided) stream deposits (High & Picard, 1974; Miao et al., 2008). The average PC trend indicate an entry point in the eastern basin, whereas the western basin may have been less confined, as suggested by the greater PC divergence combined with scattered sandstone channel facies in between (eroded) fine-grained floodplain deposits.

The Red Qahlah members show a radical change in azimuth direction to an average northerly trend, perpendicular to the Range-front fault (Figure 10b). Individually, measurements have a large spread from NE to NW but with
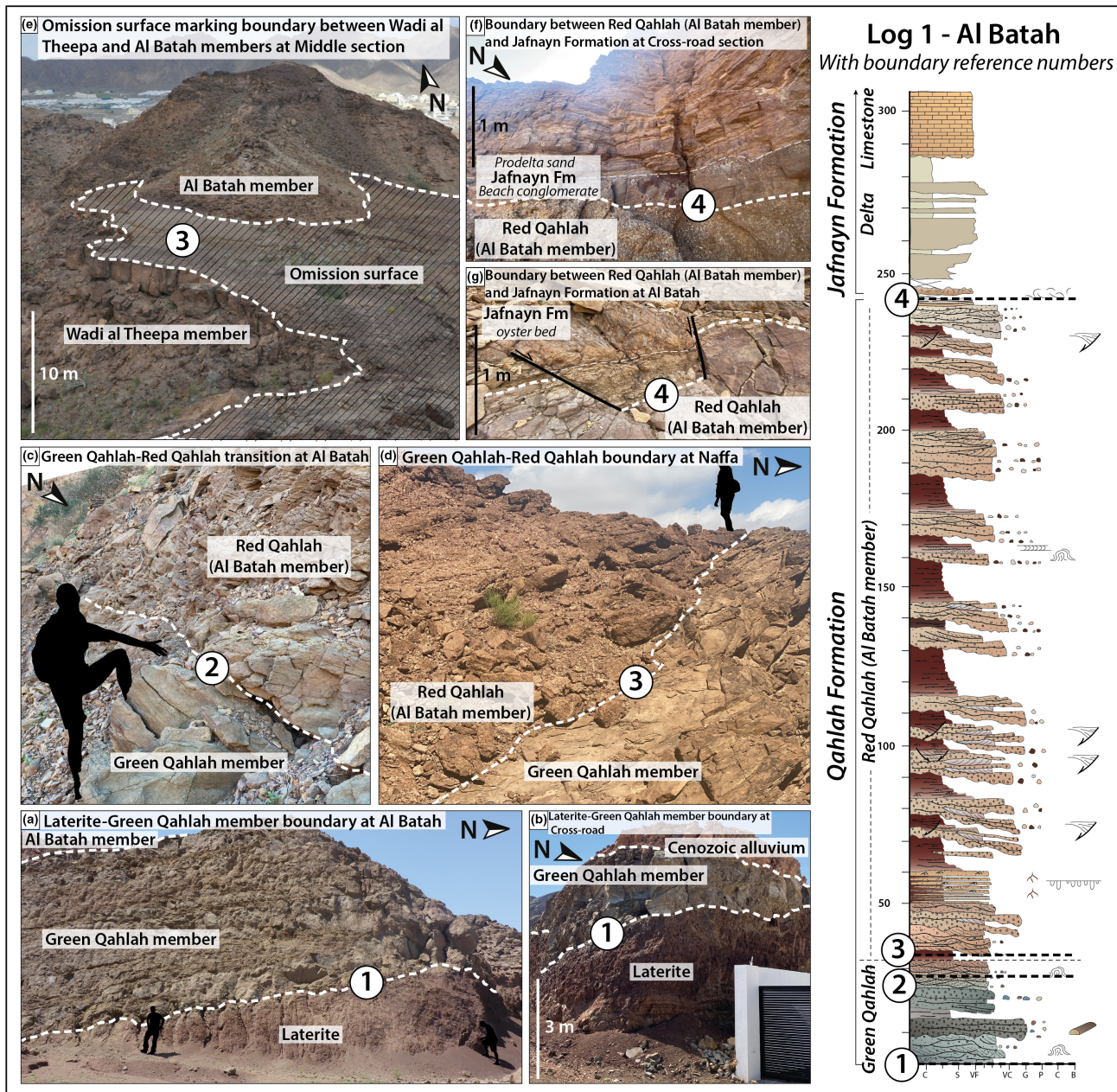
FIGURE 14 Boundaries between formations and members in the Fanja Basin. (a,b) The sharp, erosive boundary between the laterite at Al Batah (a) and at the cross-road section (b). In the latter, the green Qahlah member is erosively overlain by red alluvium of tertiary age. (c) The colour transition from green to red marking the gradual transition in mineralogy between the green and red Qahlah members and marking the pinchout of the Wadi al Theepa member in the eastern Fanja Basin at Al Batah. (d) The sharp lithological boundary between the green Qahlah member green fluvial sandstones and Al Batah member red alluvial conglomerates at Naffa. (e) The striking omission surface at middle section marking the pinchout of the Al Batah member into the Wadi al Theepa member in the western Fanja Basin. (f,g) The unconformable boundary between the Qahlah Formation and overlying Jafnayn Formation. At the cross-road section (f) this is a sharp contact between alluvial conglomerates of the Al Batah member and wave reworked sandstones again sharply overlain by prodelta sand and silt. At Al Batah (g), the boundary is a sharp, faulted contact between red alluvial sandstones of the Al Batah member and marine siltstone with abundant oyster shells. See the log (Al Batah) to the right for location of the different boundaries in the succession (numbered). Refer to Figure 3a for locations and Figure 2 for log legend.

dominating north trend in the Al Batah member, northwest in the central basin (Middle section) and NNE in the Wadi al Theepa member (Figure 10b). The perpendicular trend to

the Range-front fault with a crescent spreading is indicative of alluvial fans, which develops from water-gaps in the immediate footwall (Blair & McPherson, 2009). The facies belt

analysis substantiate spreading in a crescent shape out into the hanging-wall (Viseras & Fernández, 1994).

4.6 | Mineralogy

The mineralogical observations elaborated in this section are summarised in Figures 4 and 5.

4.6.1 | Mineralogical character of the Green Qahlah member

4.6.1.1 | *XRD bulk analysis of sandstones and conglomerates*

The Green Qahlah member sandstones show an abundance of quartz and chlorite, together comprising 83%–97% of the bulk (Figure 4). Microcline occurs in minor amounts (1%–3%). One sample contains 7% muscovite/illite, >2% pyroxene, 4% rutile and >2% haematite. Kaolin minerals are absent throughout the section. Traces (>1%) of goethite was recorded in one sample, but this mineral is otherwise absent. The only carbonate mineral detected is calcite (>1%–14%).

4.6.1.2 | *Thin section and SEM analysis*

The sampled Green Qahlah member sandstones contain sub-angular to rounded grains of very fine- to medium-grained sandstone (Figure 5a). An intermedial to good sorting and a low to medium degree porosity characterises most samples. The preponderant silica component occurs mainly in the form of monocrystalline quartz grains (55%), secondarily in polycrystalline quartz grains (8%), and sporadically in chert grains (1%), which appears to become more abundant stratigraphically upwards. Lithic rock fragments are abundant (20%) and often occur as larger clasts than the average monocrystalline quartz grains. The lithic clast portion is enriched in mafic elements (e.g. Fe and Mg), potassium and igneous minerals (e.g. pyroxene) and metamorphic minerals (e.g. Spessartine garnets). Feldspar grains are few (<2%) and unweathered, whereas sparsely occurring micas (e.g. Muscovite/Illite) (<2%) occur as smeared particles between grains. The remaining minerals traced in the XRD analysis occur together with a large proportion of the mafic and igneous minerals as cement. The cement may either be dominated by Calcite, Iron or Magnesium (Figure 5a).

4.6.2 | Mineralogical character of the green-red transition

4.6.2.1 | *XRD bulk analysis of sandstones and conglomerates*

Three out of four samples from the green/red transition display a mixture of the green and red mineralogical assemblies, with both chlorite (5%–7%), goethite (2%–3%) and kaolinite (12%–13%) represented (Figure 4). These samples also contain ankerite (7%–8%) and traces of calcite, whereas dolomite is absent. The fourth sample is dominated by quartz (70%) and kaolinite (19%) with minor haematite (2%). Herein, chlorite is absent and ankerite replaced by dolomite (5%), and the fourth sample thus shares mineralogical characteristics with the Red Qahlah above (Figure 4).

4.6.2.2 | *Thin section and SEM analysis*

At the green-red transition, a poorer sorting, larger grain size (fine- to very coarse-grained), and higher grain-angularity characterises the samples. The silica-component occurs predominantly in the form of polycrystalline quartz and chert with a lesser amount of monocrystalline quartz. The lithic rock fragment portion is lower than in the Green Qahlah (<15%), but still forms a significant component of the bulk. Ferric minerals (e.g. Chlorite, Haematite, and Ankerite) and Calcite are concentrated mainly as cement. The increased Kaolinite content documented in the XRD (Figure 4) occurs both as pseudomorphs (dissolved grains) and as pore-filling cement.

4.6.3 | Mineralogical character of the red Qahlah

4.6.3.1 | *XRD bulk analysis of sandstones and conglomerates*

The most abundant minerals in the Red Qahlah samples are quartz and kaolinite, accounting for 74%–94% of the bulk samples (Figure 4). The carbonate mineral assemblage is more diverse in the Red Qahlah, where dolomite and ankerite are the most common phases. Together with minor amounts of calcite (1%–2%), these carbonate minerals account for 1%–17% of the bulk. The remaining bulk is composed largely of goethite (2%–3%), muscovite/illite (2%), calcite (1%–2%), and haematite (averagely 1% except one sample with 6%), with traces of microcline and chlorite in some samples. No traces of igneous minerals (e.g. pyroxene, amphibole, and epidote) were encountered.

4.6.3.2 | *Thin section and SEM analysis*

The Red Qahlah samples exhibit very poor sorting with grains ranging in size from very fine to very coarse-grained with a high grain angularity. Kaolinite fills the pore space and most likely reduced any former porosity significantly (Figure 5b). The high silica content in the Red Qahlah is mainly concentrated in (radiolarian) chert grains (>60%) and minor amounts (<5%) in the form of poly- and monocrystalline quartz. The remaining minerals

inferred from the XRD (Figure 4) are mainly concentrated in cement, dominated by Iron, Calcite and Magnesium (Figure 5b).

4.6.4 | Mineralogical character of mudstones (XRD)

Among the three mudstone samples collected from the Qahlah Formation, kaolinite is the dominating clay mineral. Chlorite, and possibly interstratified chlorite/illite, were also detected in the lowermost mudstone sample. Silica occurs in all three mudstone samples.

5 | DISCUSSION

The Fanja Basin represents an excellent opportunity to study how a small basin develops during early stages of extension as reflected by (i) basin-scale growth-faults and folds representing synclines and anticlines that link to fault-segments of higher- and lower displacement, (ii) basin internal faults and bedding-scale growth wedges, (iii) vertical and lateral variations in sediment infill-patterns, and (iv) lateral mineralogical changes reflecting a provenance shift. Linked with the contemporaneous changing drainage directions, fault-displacement, and facies changes, the observations interweave a development-story for the Fanja Basin linked to the growth of fault segments in the Range-front fault. However, the timing of segmented basin growth and exact correlations remains an issue to resolve due to limited age-restricting data. Scattering of outcrops and extensive faulting and folding further challenges correlation and localisation of formational boundaries. Furthermore, as stratigraphy is only preserved in immediate proximity to the Range-front fault, distal basin deposition necessitates conceptual explanation. The reasoning for conclusions of fault-timing and sedimentary response, and potential evolution scenarios is discussed in the following sections.

5.1 | Rift-basin development stages

5.1.1 | Pre-rift: The laterite member

The varying thickness and laterally discontinuous distribution of the lateritic basal Qahlah Formation (Figure 7) is a common trait of basal terrigenous sequences resting directly on a topographically complex unconformity (Nolan et al., 1990). The distribution of the laterite does not necessarily coincide with the location of fault-bounded basins (Alsharhan & Nasir, 1996), and probably reflects deposition in a pre-rift, rugged ophiolite landscape. Weathering profiles distribution was controlled by topography, and most likely, the laterite-rich horizons were better preserved in the topographic lows of the ophiolite surface. Higher ground became selectively eroded (e.g. Thorne et al., 2012), with sediment transport towards the lowest point in the landscape, being rerouted around topographic highs on the way. This pattern conforms well to an early-rift scenario (Gawthorpe & Leeder, 2000; Smyrak-Sikora et al., 2019, 2020, 2021) and, further acknowledges the observation of fault-bound growth-sections in the overlying Green Qahlah member.

5.1.2 | Rift initiation: The Green Qahlah member

The localised occurrences of deposits of the Green Qahlah member in fault-bounded basins (i.e. Fanja and Saʹal basins; Figure 1), combined with axially trending drainage (Figure 10a), verify that faulting had initiated when this unit was deposited (Prosser, 1993; Würtzen et al., 2022) (Figure 15). Faulting ascribes to orogenic collapse by extension in the Maastrichtian-Palaeocene, when faults above detachments exerted control on local topography and localised vertical movements. As tectonic domes evolved, faulting focused on dome-margins, such as the Range-front fault (Braathen & Osmundsen, 2019). The Fanja Basin records some of this evolution. Generalised models of rift evolution forecast an initial stage of extension, in which pre-existing drainage trends will prevail but start to modify as uplifted footwalls next to down-faulted depressions evolve in the landscape (e.g. Smyrak-Sikora et al., 2019). Substantially deep drainage basins in footwall regions had not yet developed, as mirrored by the confined alluvial fan deposits within the Green Qahlah member in the east, in Fault Valley (Figure 7), representing small fan cone deposits along the fault scarp (Figure 16a). The interaction with fine-grained thick deposits in this location (Figure 12e) suggests that these fans dispersed into wet substrate westward, such as a shallow lacustrine or swamp environment in the immediate hanging-wall (Figure 8a). Shallow lakes commonly develop in structurally isolated half-grabens during the earliest stages of rift evolution as seen for example in the East African Rift system (e.g. Chorowicz, 2005).

The laterally discontinuous distribution and varying thickness of Green Qahlah member deposits within the Fanja Basin might reflect depositional troughs from
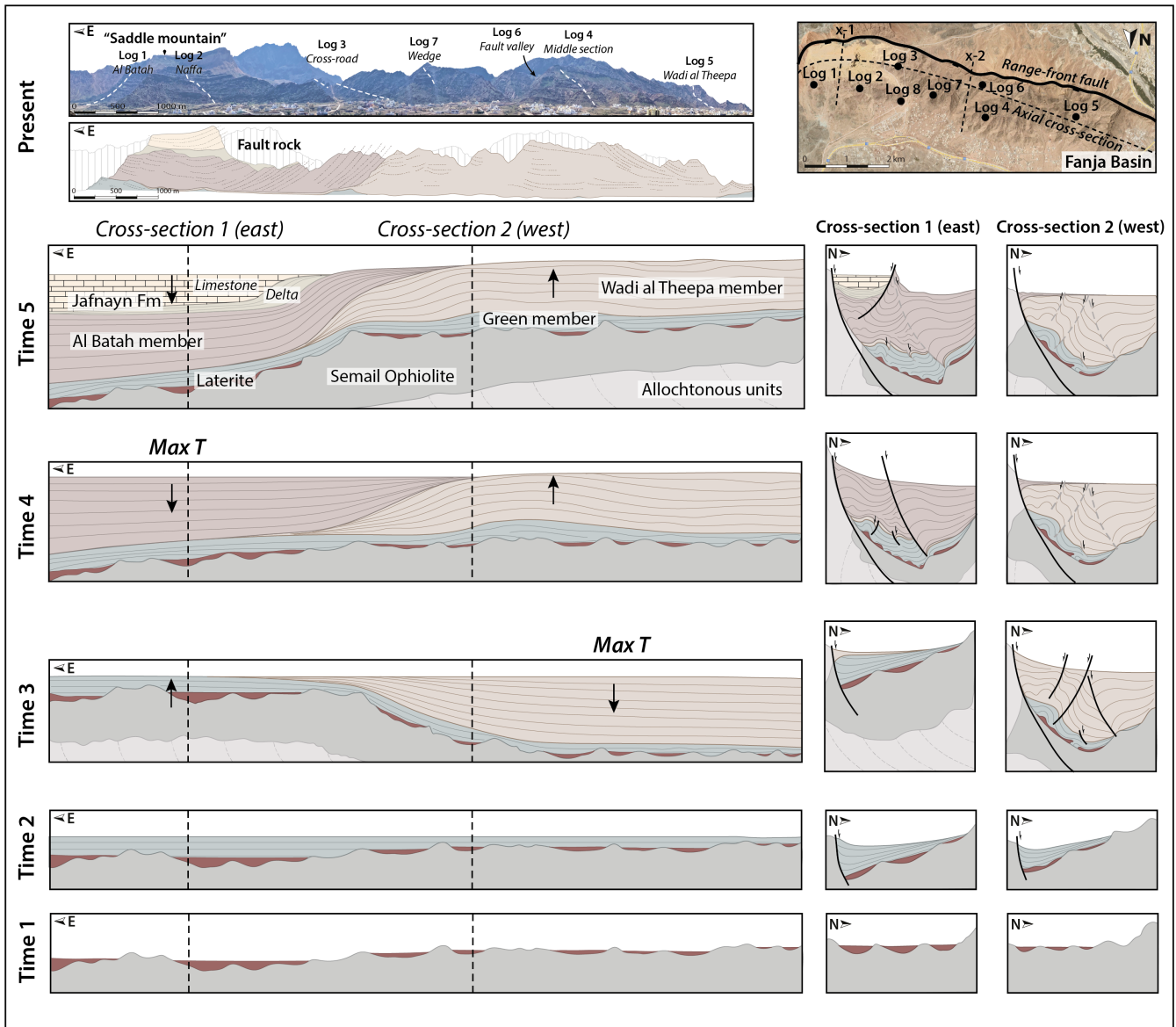
FIGURE 15 Summary of step-wise basin development at times of deposition for each stratigraphic unit up until the present-day configuration presented in E-W fault-parallel panel and S-N fault-transverse cross-sections. Max-throw (max-T) location along the range-front fault is marked for the units at time 3 (Wadi al Theepa member) and time 4 (Al Batah member). In the cross-sections, the internal faults are estimated and not to be scaled. The location of the cross-sections and logged sections are marked on the inset mapper in the upper right corner.

persistent inherent topography in the underlying sur-face (Figure 15; Opluštil & Vízdal, 1995). Alternatively, sediment routing into the basin from the footwall of the Range-front fault took place through gaps or relays during early, low-displacement fault evolution. With the two areas of thicker Green Qahlah corresponding to two jogs in the fault, indicative of former segment-linkage areas, there appears to be inherited fault control on the early basin evolution. In any case, scattered sandstone ridges in the modern valley reflect channel sandstone deposits, whereas the areas in between mimics localised erosion that favoured zones of more erodible fine-grained deposits

(Moosdorf et al., 2018; Williams et al., 2011). Thus, we consider the distribution of Green Qahlah member sand-stones to reflect the position of concentrated channel ele-ments, which dominated in the east. Western valley floor areas that exhibit scattered Green Qahlah member sand-stone ridges reflect areas that were dominated by flood-plain fines and secondarily scattered channel elements (Figure 8b; Williams et al., 2011). This provides an image of initial stages of regional faulting, with entry-point for sediments proximal to early fault-gaps or relay zones, the main one being near the eastern large jog in the Range-front fault (Figures 3a and 10).
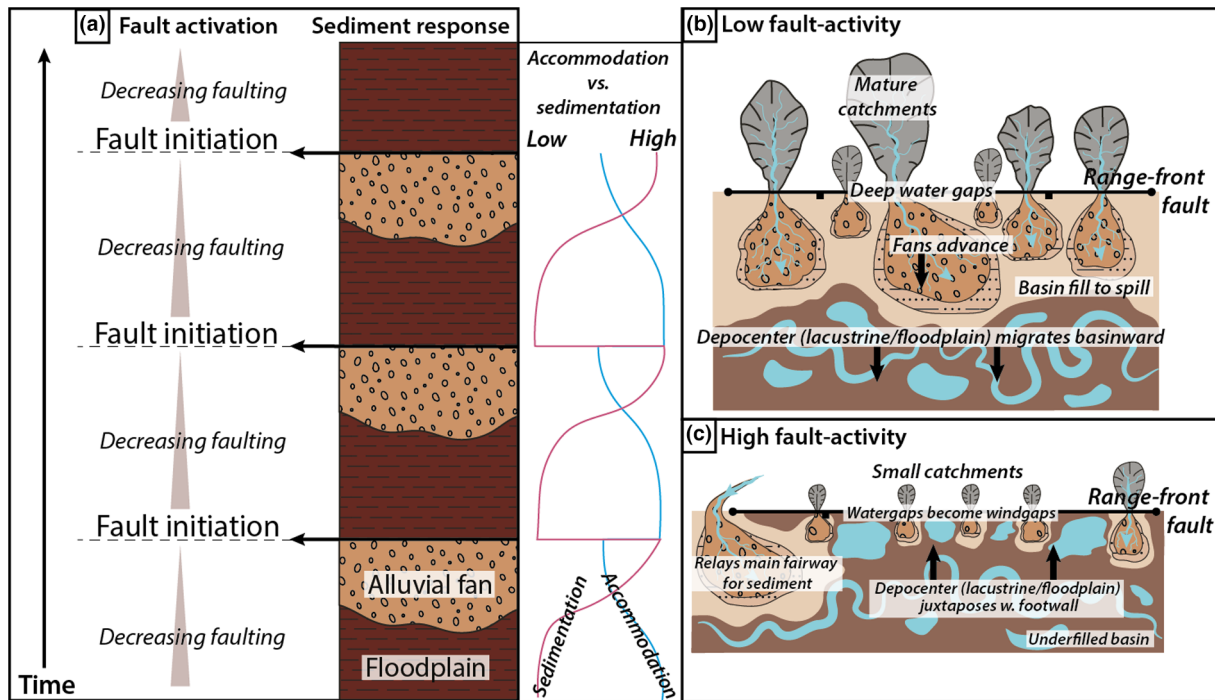
FIGURE 16 A conceptualised illustration of the fault-timing theory for the red Qahlah members. (a) With time on the *Y*-axis, it is illustrated how fault movement initiate deposition of fine-grained units, which may be thick, depositing during the interval of accommodation creation, followed by deposition of coarse-grained alluvial units, marking the decrease of fault activity. This is linked up towards cycles of high versus low accommodation and sedimentation. (b) Basin setting during low fault-activity in the Fanja Basin. The landscape degrades as catchments mature and alluvial fans advance out into the basin, resulting in the retreat of basin plain deposits such as lacustrine and floodplain deposits to more distal locations. (c) Basin setting during high fault-activity in the Fanja Basin. Topography increases due to footwall uplift and outpaces catchment degradation. Consequently water-gaps might become wind-gaps and cut off sediment input, so that the basin becomes under-filled. The sediment input is redirected into relays, which act as the main fairways of sediment. Alluvial fans retreat, and lacustrine and floodplain deposition juxtaposes with footwall.

5.1.3 | Western syn-rift phase: Wadi al Theepa member (Red Qahlah)

Concerning the Red Qahlah, significant changes in bedding dip (Figure 15), a noticeable increase in fine-grained interbedded facies towards the east, coupled with PC observations (Figure 10b), endorse two fan complexes building out from the southern footwall and across the Range-front fault. These fan complexes were sourced from water-gaps in the Range-front allowing sediment transport through the uplifted footwall crest (Figure 16b). Between the fans, a gentle N-S-oriented orthogonal syncline adjoins a gentle bend in the fault, ascribed to two former curvilinear fault segments (Figure 3a). Overall, this pattern is suggestive of maximum fault throw (Tmax) in the west during deposition of the Wadi al Theepa member, with minimum throw towards the east where it wedges to a minimum (Figure 15). T-max on the fault during deposition of Wadi al Theepa member was likely accumulating on the segment behind Wadi al Theepa (Figure 15), as this coincides with the thickest measured section in the western

part of the basin (Figure 7). The dominance of immature coarse-grained sediment with a high concentration of gravity- and hyperconcentrated flow facies in the fault-proximal and western sections (Figure 7) points to an inner to medial fan zone (Blair, 1999b; Gao et al., 2020; Sohn et al., 1999), consistent with a high sedimentation rate (S) relative to the rate of accommodation (A) (Huerta et al., 2011; Rogers et al., 2016). Despite the low percentage of fine-grained interbeds in the western section (Figure 7), the thickness of the succession conforms to considerable accommodation creation. During low A/S, subsidence variations are considered to have minor effects on alluvial architecture and facies development (Hickson et al., 2005). Besides, if sediment input exceeded the accommodation creation, the formation of deep and long-lasting standing-water bodies may have been prevented (Huerta et al., 2011; Rogers et al., 2016), confirmed by our data in the western section (Figure 7). On a different note, fluctuations in climate with drier conditions during deposition of the Wadi al Theepa member could also result in a more sand-rich succession due to increased mechanical weathering (Nystuen

et al., 2014; Würtzen et al., 2022), minor formation of fine-grained deposits due to dry-out of the system, and a possible prevalence of transverse over axial sedimentation (Fordham et al., 2010). Climatic studies suggest two global warming events in the Maastrichtian (Abramovich et al., 2010) overall humid seasonal to perennial but with one dry seasonal period recorded in the Late Maastrichtian (Abramovich et al., 2003; Adatte et al., 2005; Keller, 2004). This arid climate event could potentially correlate with the Wadi al Theepa member.

5.1.4 | Eastern syn-rift phase: Al Batah member (Red Qahlah)

The Al Batah member is located to the east, in a distinct orthogonal synclinal basin rooted in the major jog of the Range-front fault (Figure 3a). An anticline in the eastern basin end (Figure 3), where the ophiolite is juxtaposed with the fault, is considered the expression of a former low-displacement relay ramp in the area. On the other side, the western boundary of the Al Batah sub-basin is expressed as a gentle orthogonal monocline in the Wadi al Theepa member. There, the Al Batah member abruptly wedges out and upper beds of the Wadi al Theepa member are truncated along omission surfaces (Figure 15). At this stage, the basin configuration conforms to significant focusing of throw accumulation on the major jog in the Range-front fault, consistent with segment linkage/breaching and subsequent focused throw on the former linkage area.

The lesser amount of gravity-flow deposits (FA1) relative to hyperconcentrated- and stream-flow deposits (FA2) in the Al Batah member compared with the Wadi al Theepa member (Figure 7) is consistent with different, possibly interplaying, scenarios. Firstly, a higher accommodation rate relative to the rate of sedimentation prevailed during deposition, as is necessary for the preservation of such thick mudstone intervals in continental basins (Würtzen et al., 2022). Secondly, several trends (e.g. higher maturity, better sorting, more distal facies, thicker, more continuous floodplain deposits in between conglomeratic units; Figure 7) in the eastern section can be ascribed to deposition in the medial to outer zone of alluvial fans (Blair, 1999b; Gao et al., 2020). The sediment must have had a larger transport distance from the source, which coincides with the presence of an initial relay ramp in the eastern end of the basin, suggested from the jog in the range-front fault at this location (Figure 3; Peacock & Sanderson, 1994; Rotevatn et al., 2007). A water-gap would have established as the relay was rejuvenated, creating a source for sediments. Further, recycling of older fan sediments from the

uplifted Wadi al Theepa member (Figure 15) may have added to the improved sorting of the Al Batah member conglomerates. A provision of sediment from west is supported by palaeocurrent trends in the Al Batah member, which show a large spread with some measurements indeed trending eastward (Figure 10b). A more humid climate than during deposition of the Wadi al Theepa member could also inflict conditions resulting in more water-laid flows and higher concentration of mudstone (Moscariello, 2018; Nystuen et al., 2014). Besides, during increased humidity, chemical weathering will prevail in the hinterland, favouring the production of clay over sand (Nystuen et al., 2014). Palaeoenvironmental studies of Late Maastrichtian rocks of Israel, Madagascar, and Tunisia document a warm-humid period in the latest Maastrichtian (Abramovich et al., 2003, 2010; Keller, 2004).

5.1.5 | Graben-formation: Jafnayn formation

Geometrically, the Jafnayn succession is bound by south and north-dipping faults on opposite sides, setting up a symmetric graben (Figure 15). A basal transgressive lag followed by a southeast-building deltaic succession in the lower Jafnayn Formation show that the latest(?) Maastrichtian to Late Palaeocene hiatus was transgressed, likely from the southeast in what could have been a fjord-style basin. This part of the basin evolution is however outside the scope of this contribution and will therefore not be further entertained.

5.2 | Punctuated faulting and depositional response

According to Gao et al. (2020), (ephemeral) alluvial fans commonly develop through stages of lobe building, channel building and abandonment. The lobe building stage is characterised by sheet- and unconfined stream-floods, and surficial ponds on the distal fan, whereas the channel building stage is characterised by the development of gravelly stream-flows. During the abandonment stage, surficial secondary processes, like wind and overland flows, are dominant (Gao et al., 2020). The Red Qahlah fans were likely of perennial type, according to climatic studies (e.g. Keller, 2004), and as such, the frequency of flood discharge events may have been high and the intermittent periods of inactivity low, compared with ephemeral alluvial fans phases. These phases of lobe-building and -abandonment produce recognisable boundaries and facies sets, which are strongly linked to fault movement and accommodation creation (Figure 16a). During increased

fault linkage, and the connected merging- and enlargement of drainage basins, drainage is redirected into the catchments (Mather et al., 2000). Clevis et al. (2003) shows that sediments may be captured for tens to hundred thousand years in catchment areas before being dispersed into the basin thus advocating that periods of fan progradation happen long after termination of localised faulting, whereas times of active faulting are characterised by retrogradation of gravel lobes and thus more widespread deposition of finer-grained sediment. This suggests that fault events in the Fanja Basin coincide with the sharp boundary between conglomeratic units and overlying overbank deposits (FA5 and FA6) (Figure 7). This scheme is supported by (i) the rapid creation of accommodation reflected by the sharp shift into fine-grained successions, often of significant thickness (Figures 7 and 13), (ii) the abundant presence of small-scale faults in the conglomerate top surfaces, hosting metres thick sub-depocentres filled with growth packages in FA5 and FA6 (Figure 6b,c), which furthermore show abundant convolute bedding and load structures, indicative of syn-depositional seismicity (Figure 11e; Evans, 1991), and (iii) how surfaces of significant facies shifts may appear sediment starved, supported by the presence of duricrusts (Facies R; Table 1.3) (Blair & McPherson, 2009). Accommodation likely outpaced sedimentation during the active faulting, and these rapidly created depocentres commonly accumulated fine-grained sediments (e.g. Prosser, 1993). This is especially expected under perennial conditions, where chemical weathering produce abundant clay particles (Nystuen et al., 2014), which settle through suspension and form thick mudstone units, as noticed in the Red Qahlah members (Figure 13).

Periods of faulting are short relative to episodes of increased tectonic activity (e.g. Embry et al., 2019). The deposition following faulting may for extended periods happen through suspension settling of fine-grained lithologies until the uplifted footwall crests are cut by water-gaps through which coarse sediment fill the basin (Clevis et al., 2003). Periods of low fault activity thus result in landscape degradation and fan advance as gradually more mature composite catchments carry more water and sediment into the basin (Figure 16b). The lower topographic gradients during these periods may also lead to the basin being overfilled which show in the stratigraphic record as coarsening upwards (Prosser, 1993). Oppositely, during periods of high fault-activity, water-gaps may sustain near fault-tips, but more commonly become wind-gaps to small catchments, as the footwall is uplifted, and relays become the main fairways for sediment input (Figure 16c; Densmore et al., 2009; Friedmann & Burbank, 1995). The landscape-building and resulting cut-off of water-gaps

means that the basin may have been periodically underfilled (Gawthorpe & Leeder, 2000; Prosser, 1993), conforming to the observation that omission surfaces followed by overbank fines (Figure 7) represent long-time intervals of low fault-activity (Figure 16c). The coarse-grained intervals in the Red Qahlah members thus represent the end of each fault cycle, before initiation of new fault movement and renewed deposition of fine-grained deposits (Figure 16a).

Climatic fluctuations have also been documented to control fan aggradation/incision by Terrizzano et al. (2017), who correlated these events to periods of climatic instability (mainly transitions from wet to dry conditions) with only local aggradation/incision being linked to a tectonic component. The more cyclic deposition with longer periods of low sediment supply in the Al Batah member compared with the Wadi al Theepa member could relate to a strong climatic control with fluctuations where the floodplain dominated (Sadler & Kelly, 1993).

5.3 | Palaeoclimate

Published palaeoclimate studies generally agree that a tropical climate prevailed at equatorial latitudes during the Maastrichtian, based on biostratigraphy (Schlüter et al., 2008), palaeosol analysis (Kumari et al., 2021), and palynology (Mishra et al., 2022). In the Qahlah Formation of the Fanja Basin, this is supported mineralogically, first of all by the presence of laterite, which reflect chemical weathering of exposed surfaces and near-surface rocks during tropical-subtropical conditions (Al-Khirbash, 2020; Nolan et al., 1990). The high proportion of chlorite in the Green Qahlah member (Figure 4) is, however, somewhat contradicting, as chlorite weather easily and transform into other clay minerals, e.g. smectite, under tropical conditions (Garzanti et al., 2014). Chlorite may though also stem from alterations of weathered mafic/ultramafic minerals, which is not uncommon in tropical climates (van de Kamp & Leake, 1995). The large concentration of kaolinite cement in the Red Qahlah members (Figures 4 and 5b) further conforms to a warm climate with high constant precipitation (Garzanti et al., 2014). Stable humid conditions are also inferred from the prevalence of goethite in each of the Red Qahlah members, which forms through weathering of iron-rich minerals that concentrate in soils of swamps and lakes (Brenko et al., 2020). As a consideration, not readily identified in our data, there are variations in the overall tropical climate in the Maastrichtian Tethys Sea with alternating seasonal to perennial humid periods and a seasonally dry period in the Late Maastrichtian (Keller, 2004).

5.4 | Provenance

The transition in mineral assemblage from Green Qahlah to Red Qahlah (Figure 4) resembles an inverted mineralogical stratigraphy of the regional tectonostratigraphy, as encountered around the Saith Hatat and Jabal Akhdar domes with surrounding thrust-nappe rocks, with early basin fill sourced from structurally higher nappes (Abbasi et al., 2014; Bauer et al., 2018; Mattern et al., 2020; Mattern & Scharf, 2018; Searle, 2019).

5.4.1 | Green Qahlah member and laterite member

The high Ni-concentration previously recorded in the laterite (Al-Khirbash, 2020) matches the mafic/ultramafic protolith in the Semail Ophiolite, which overall encompasses harzburgite (mantle sequence), dunite and wehrlite (Moho transition zone), and gabbro (crustal sequence) (Dilek, 2003; Searle, 2019). The mafic/ultramafic composition of the ophiolite is also reflected in the bulk mineralogy of the Green Qahlah member, reflect in the high concentrations of chlorite and other ferric minerals, and traces of pyroxene (Figure 4). Chlorite is a common alteration product of olivine and pyroxene during intensive weathering of ultramafic to mafic igneous rocks (van de Kamp & Leake, 1995). These minerals are abundant components in the peridotites (e.g. Harzburgite and Dunite) and gabbros surrounding the Fanja Basin (Figure 1; Tamura & Arai, 2006), and the Semail Ophiolite is therefore counted as the main source for the Green Qahlah sediments (Figure 17c). The large content of monocrystalline quartz crystals indicates an additional metasedimentary/quarzitic source. Quartz appears in a wide spectre of rocks and there are several potential sources in the Al Hajar Mountain stratigraphy that could have provided quartz; the abundant metasediments in the thrust-nappes below the ophiolite (i.e. Hawasina) represent the most obvious source (Figure 1). The Amdeh and Hatat formations quartzites and schists (Mattern et al., 2020) have been evaluated as potential sources, but uplands for Maastrichtian sediments in the domes are contested by the fact that these rocks overall started uplift from deep, metamorphic levels in the Maastrichtian and approached the surface in the Eocene (Hansman et al., 2017). The garnets in the Green Qahlah may indicate sourcing from garnet-amphibolite and schist in the metamorphic sole of the ophiolite (Gnos, 1998; Gray et al., 2004; Searle & Cox, 2002; Warren & Waters, 2006), which at present time is exposed just south and east of the Fanja Basin (Figure 17a).

5.4.2 | Red Qahlah members

The striking change in mineralogical composition between the green and red Qahlah (Figure 4) reflects a shift in source unit, probably as a consequence of significant change in basin configuration with new sediment entry-points (Figure 17). The predominance of radiolarian chert in the bulk of the Red Qahlah members (Figure 5b) verifies a source in the Hawasina Nappe Complex (Blechschmidt et al., 2004). A thin sliver of Hawasina radiolarian chert outcrops around the western edge of the Saih Hatat dome, along with patches in the footwall to the Fanja Basin (Figure 17a). Footwall uplift during faulting next to the Fanja Basin would have uplifted the stratigraphy underlying the ophiolite (i.e. the Hawasina complex) making this succession an available source for sediments. Combined with the PC directions radiating outwards directly from the footwall of the basin (Figure 10b), it seems plausible that footwall uplift would have exposed the Hawasina stratigraphy to erosion and subsequent transport into the Fanja Basin. Additional source units providing chert may include the Muti Formation forming part of the Hajar Supergroup, which stratigraphically underlies the Hawasina nappe (Figure 2), and is exposed just ESE of the Fanja Basin (Figure 17a). It may have been exposed during unroofing of the Saih Hatat dome and presented a source unit, at least for the Al Batah member (Figure 17b). Abbasi et al. (2014) indicates that an increasing amount of carbonate content upwards in the Fanja Basin stratigraphy reflects material derived from the Hajar Supergroup limestones. However, carbonates are abundant throughout the Al Hajar Mountains stratigraphy (Figure 1). Source units north and east of the basin during deposition of the Al Batah member are consistent with the PC measurements in the eastern part of the basin, trending NW, and supported further by the presence of a relay ramp in this area, which would have been a major sediment pathway into the basin at that time.

6 | CONCLUSIONS

This study documents for the first time the tectonostratigraphic development of the Late Cretaceous Fanja continental half-graben basin (northern Oman). The observations provide valuable insights into how extensional fault and fold growth impact accommodation development, drainage patterns, and sedimentary infill in continental half-graben basins by combining structural, sedimentological, and mineralogical analyses. The main findings of the study are summarised as follows:
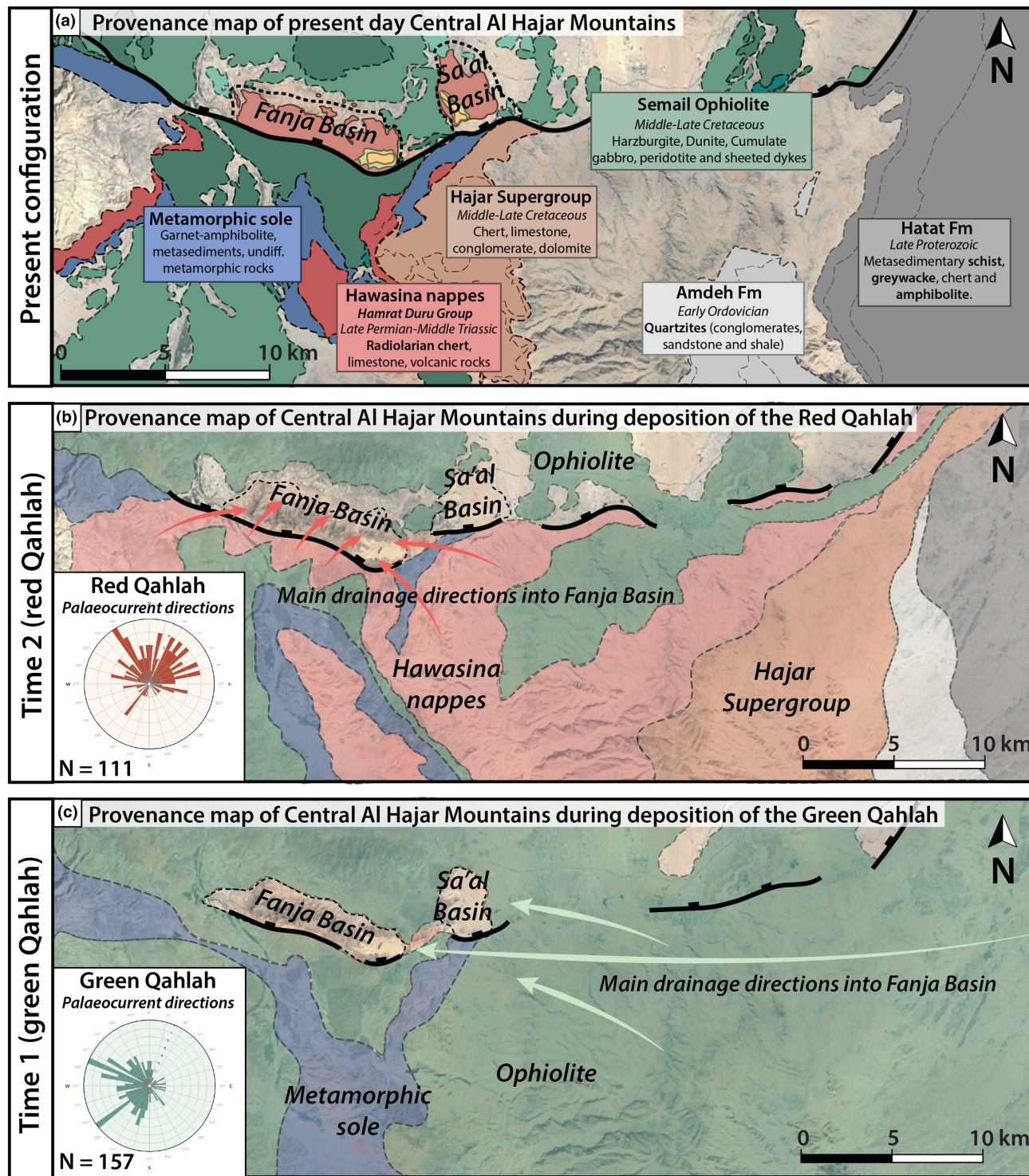
FIGURE 17 (a) Map of the central Al Hajar Mountains and Fanja region with relevant provenance units' distribution marked in their present-day location with main lithologies summarised for each. The drainage directions (Figure 10) for each member indicate approximately from which direction the sediments were sourced through time and combined with vertical mineralogical variations through the sections, the source units can be pin-pointed. During deposition of the green Qahlah (c), sediments where sourced mainly from the ophiolite surface, which covered the Al Hajar Mountains. Metasediments of the metamorphic sole might have been exposed around the Al Hajar Mountains and represent a contributory source unit. The red Qahlah members (b) were sourced mainly from the Hawasina nappe complex as the Semail Ophiolite cover had been largely eroded in the interior Al Hajar Mountains. The Hajar Supergroup might have been exposed too, at least in the central domal structures, representing an additional source. The sediments were transported into the basin across the Range-front fault from south to north and from an eastern inlet (relay section). Furthermore, the Range-front fault footwall uplift exposed underlying allochthonous units in the footwall to the Fanja Basin.

1. Evolving displacement gradients, especially at the breaching-point of relay zones, form fault-orthogonal folds, which control basin accommodation and hence fillarchitecture, as evidenced from observations along the Range-front fault and contemporary infill in the Fanja Basin.

2. The Red Qahlah is sub-divided into two members, the lower *Wadi al Theepa member*, concentrated in the west, and the upper *Al Batah member*, concentrated in the east. The distinction is based on a noticeable reduction in fine-grained interbeds towards west wedging onto former conglomerates of the Wadi al Theepa member in a gentle fault-orthogonal monocline.

3. Changes in facies type and distribution, mineralogy and bedding geometries in combination with structural observations reflect transitions in rift phases. In the Fanja Basin, the dataset documents the evolution from an early to mature rift through five phases: *pre-rift phase* (Laterite member), *rift-initiation phase* (Green Qahlah member), *western syn-rift phase* (Wadi al Theepa member), *eastern syn-rift phase* (Al Batah member), and *graben formation* (Jafnayn Formation).

4. Continental rift basins commonly fill initially by axially draining braided streams (i.e. *Green Qahlah member*) during the early rift phase where the basin has low-relief, and later during the syn-rift phase by footwall sourced alluvial fan deposition (i.e. *Red Qahlah members*) as footwall relief increase in response to focused fault-movement. During growth and linkage of basin bounding fault-segments, the Tmax may shift between segments, as in the Fanja Basin where locus shifted from a western- to an eastern fault segment.

5. The timing of alluvial fan dispersal may be strongly controlled by faulting as the footwall is lifted and catchments evolve to deliver sediment, exemplified by the cyclic interbedded fine and coarse-grained units in the Al Batah member. Fault-initiations may be marked by omission surfaces in tops of conglomerates overlain by thick floodplain fines, reflecting accommodation outpacing sedimentation in the rift climax. Outbuilding of alluvial fans finalises each fault-cycle, represented by amalgamated coarse-grained intervals.

6. Smaller growth-faults (characterised by infill of fine-grained sediments into metre-sized fault-bounded 'micro-basins') in conglomerate tops at the boundary between these and thick fine-grained floodplain units reflect the initiation of faulting-events. These horizons conform to the shift in depositional setting from coarse alluvial fans prograding into an overfilled basin to sudden accommodation creation and footwall uplift resulting in A>S and an underfilled basin filled by lacustrine and floodplain deposits.

7. Climatic fluctuations may strongly influence facies distribution by affecting weathering patterns in the hinterland and thereby the sand: mud ratio in the sediment input. In the Fanja Basin, a tropical climate, as documented in climatic studies, is reflected in facies-indications for high run-off rates as well as in the mineralogy, which is rich in goethite and kaolinite.

8. Sediment provenance may change with the evolution of a basin-bounding fault, such as the Range-front fault in the Fanja Basin, suggesting unroofing of the footwall in conjunction with fault-driven topography-enforced sediment routing. This is recorded in the Fanja Basin through mineralogical analysis, which shows a distinct change from the quartz and lithic (ophiolite) detritus dominating the Green Qahlah to the chert, kaolinite and dolomite-dominated Red Qahlah. Combined with palaeodrainage trends, a potential source for the Green Qahlah is evaluated to be the Semail ophiolite cover and schists of the metamorphic sole east of the Fanja Basin. The Red Qahlah was sourced mainly from the underlying Hawasina Nappe Complex, exposed in the footwall south of the basin.

The stratigraphic architecture of the Fanja continental half-graben basin reflects fault growth and dynamic depocentre-development during fill. This study demonstrates that depositional loci and resultant accumulation of depositional sub-environments are a direct consequence of this and is applicable in deterministic evaluation of a basin and its reservoirs. Linking sedimentology and fault-displacement events controlling fault-perpendicular folding, and its influence on depocentre generation and resulting stratigraphic architecture is an approach rarely considered in subsurface analysis and outcrop studies. This places the results from this study among the key outcrop-based contributions to the field.

ACKNOWLEDGEMENTS

manuscript maturation from the Tectonostratigraphic Research Group at the University of Oslo. Finally, the authors wish to thank the reviewers for their revisions of the manuscript, which improved in many ways from this.

PEER REVIEW

DATA AVAILABILITY STATEMENT

The data that support the findings of this study are available from the corresponding author upon reasonable request.

ORCID

Camilla L. Würtzen https://orcid.org/0000-0001-6715-3894
Alvar Braathen https://orcid.org/0000-0002-0869-249X
Miquel Poyatos-Moré https://orcid.org/0000-0001-7813-8868
Ivar Midtkandal https://orcid.org/0000-0002-4507-288X

REFERENCES

Abbasi, I. A., Hersi, O. S., & Al-Harthy, A. (2014). Late cretaceous conglomerates of the qahlah formation, North Oman. *Geological Society, London, Special Publications*, *392*(1), 325–341.

Abdelghany, O. (2006). Early Maastrichtian larger foraminifera of the Qahlah formation, United Arab Emirates and Sultanate of Oman border region. *Cretaceous Research*, *27*(6), 898–906.

Abramovich, S., Keller, G., Adatte, T., Stinnesbeck, W., Hottinger, L., Stueben, D., Berner, Z., Ramanivosoa, B., & Randriamanantenasoa, A. (2003). Age and paleoenvironment of the Maastrichtian to Paleocene of the Mahajanga Basin, Madagascar: A multidisciplinary approach. *Marine Micropaleontology*, *47*(1–2), 17–70.

Abramovich, S., Yovel-Corem, S., Almogi-Labin, A., & Benjamini, C. (2010). Global climate change and planktic foraminiferal response in the Maastrichtian. *Paleoceanography*, *25*(2), PA2201.

Adatte, T., Keller, G., Stüben, D., Harting, M., Kramar, U., Stinnesbeck, W., Abramovich, S., & Benjamini, C. (2005). Late Maastrichtian and K/T paleoenvironment of the eastern Tethys (Israel): Mineralogy, trace and platinum group elements, biostratigraphy and faunal turnovers. *Bulletin de la Société Géologique de France*, *176*(1), 37–55.

Al-Khirbash, S. A. (2020). Mineralogical characterization of low-grade nickel laterites from the North Oman Mountains: Using mineral liberation analyses–Scanning electron microscopy-based automated quantitative mineralogy. *Ore Geology Reviews*, *120*, 103429.

Alsharhan, A. S., & Nasir, S. J. Y. (1996). Sedimentological and geochemical interpretation of a transgressive sequence: The late cretaceous Qahlah formation in the western Oman Mountains, United Arab Emirates. *Sedimentary Geology*, *101*(3–4), 227–242.

Ashmore, P. E. (1985). *Process and form in gravel braided streams: Laboratory modelling and field observations* [Unpublished thesis]. University of Alberta.

Bauer, W., Callegari, I., Al Balushi, N., Al Busaidi, G., Al Barumi, M., & Al Shoukri, Y. (2018). Tectonic observations in the northern Saih Hatat, Sultanate of Oman. *Arabian Journal of Geosciences*, *11*(5), 1–7.

Blair, T. C. (1987). Tectonic and hydrologic controls on cyclic alluvial fan, fluvial, and lacustrine rift-basin sedimentation, Jurassic-lowermost cretaceous Todos Santos formation, Chiapas, Mexico. *Journal of Sedimentary Research*, *57*(5), 845–862.

Blair, T. C. (1999a). Alluvial fan and catchment initiation by rock avalanching, Owens Valley, California. *Geomorphology*, *28*(3–4), 201–221.

Blair, T. C. (1999b). Cause of dominance by sheetflood vs. debris-flow processes on two adjoining alluvial fans, Death Valley, California. *Sedimentology*, *46*(6), 1015–1028.

Blair, T. C. (1999c). Sedimentology of the debris-flow-dominated warm spring canyon alluvial fan, Death Valley, California. *Sedimentology*, *46*(5), 941–965.

Blair, T. C. (2000). Sedimentology and progressive tectonic unconformities of the sheetflood-dominated Hell's gate alluvial fan, Death Valley, California. *Sedimentary Geology*, *132*(3–4), 233–262.

Blair, T. C., & McPherson, J. G. (2009). Processes and forms of alluvial fans. In *Geomorphology of desert environments* (pp. 413–467). Springer.

Blechschmidt, I., Dumitrica, P., Mater, A., Krystyn, L., & Peters, T. (2004). Stratigraphic architecture of the northern Oman continental margin-Mesozoic Hamrat Duru group, Hawasina complex, Oman. *GeoArabia*, *9*(2), 81–132.

Braathen, A., & Osmundsen, P. T. (2019). Extensional tectonics rooted in orogenic collapse: Long-lived disintegration of the Semail ophiolite, Oman. *Geology*, *48*(3), 258–262. https://doi.org/10.1130/G47077.1

Brenko, T., Šoštarić, S. B., Ružičić, S., & Ivančan, T. S. (2020). Evidence for the formation of bog iron ore in soils of the Podravina region, NE Croatia: Geochemical and mineralogical study. *Quaternary International*, *536*, 13–29.

Bromley, R. G. (1975). Trace fossils at omission surfaces. In *The study of trace fossils* (pp. 399–428). Springer.

Brooke, S. A., Whittaker, A. C., Armitage, J. J., d'Arcy, M., & Watkins, S. E. (2018). Quantifying sediment transport dynamics on alluvial fans from spatial and temporal changes in grain size, Death Valley, California. *Journal of Geophysical Research: Earth Surface*, *123*(8), 2039–2067.

Brun, J. P., Sokoutis, D., Tirel, C., Gueydan, F., Van Den Driessche, J., & Beslier, M. O. (2018). Crustal versus mantle core complexes. *Tectonophysics*, *746*, 22–45.

Burns, C. E., Mountney, N. P., Hodgson, D. M., & Colombera, L. (2017). Anatomy and dimensions of fluvial crevasse-splay deposits: Examples from the cretaceous Castlegate sandstone and Neslen formation, Utah, USA. *Sedimentary Geology*, *351*, 21–35.

Calhoun, N. C., & Clague, J. J. (2018). Distinguishing between debris flows and hyperconcentrated flows: An example from the eastern Swiss Alps. *Earth Surface Processes and Landforms*, *43*(6), 1280–1294.

Chorowicz, J. (2005). The east African rift system. *Journal of African Earth Sciences*, *43*(1–3), 379–410.

Clarke, L. E. (2015). Experimental alluvial fans: Advances in understanding of fan dynamics and processes. *Geomorphology*, *244*, 135–145.

Clevis, Q., de Boer, P., & Wachter, M. (2003). Numerical modelling of drainage basin evolution and three- dimensional alluvial fan stratigraphy. *Sedimentary Geology*, *163*(1–2), 85–110.

Collinson, J. (2006). *Sedimentary structures*. Dunedin Academic Press Ltd.

Cooper, D. J. W., Ali, M. Y., & Searle, M. P. (2014). Structure of the northern Oman Mountains from the Semail ophiolite to the Foreland Basin. *Geological Society, London, Special Publications*, *392*(1), 129–153.

Dasgupta, P. (2006). Facies characteristics of Talchir formation, Jharia Basin, India: Implications for initiation of Gondwana sedimentation. *Sedimentary Geology*, *185*(1–2), 59–78.

Davies, N. S., Gibling, M. R., & Rygel, M. C. (2011). Alluvial facies evolution during the Palaeozoic greening of the continents: Case studies, conceptual models and modern analogues. *Sedimentology*, *58*(1), 220–258.

De Haas, T., Kleinhans, M. G., Carbonneau, P. E., Rubensdotter, L., & Hauber, E. (2015). Surface morphology of fans in the high-Arctic periglacial environment of Svalbard: Controls and processes. *Earth-Science Reviews*, *146*, 163–182.

de Winter, N. J., Goderis, S., Dehairs, F., Jagt, J. W., Fraaije, R. H., Van Malderen, S. J., Vanhaecke, F., & Claeys, P. (2017). Tropical seasonality in the late Campanian (late cretaceous): Comparison between multiproxy records from three bivalve taxa from Oman. *Palaeogeography, Palaeoclimatology, Palaeoecology*, *485*, 740–760.

Del Papa, C., Kirschbaum, A., Powell, J., Brod, A., Hongn, F., & Pimentel, M. (2010). Sedimentological, geochemical and paleontological insights applied to continental omission surfaces: A new approach for reconstructing an eocene foreland basin in NW Argentina. *Journal of South American Earth Sciences*, *29*(2), 327–345.

Densmore, A. L., Hetzel, R., Ivy-Ochs, S., Krugh, W. C., Dawers, N., & Kubik, P. (2009). Spatial variations in catchment-averaged denudation rates from normal fault footwalls. *Geology*, *37*(12), 1139–1142.

Dilek, Y. (2003). Ophiolite concept and its evolution. In Y. Dilek & S. Newcomb (Eds.), *Ophiolite concept and the evolution of geological thought* (Vol. *373*, pp. 1–16). Special Paper of the Geological Society of America.

Embry, A., Beauchamp, B., Dewing, K., & Dixon, J. (2019). Episodic tectonics in the Phanerozoic succession of the Canadian High Arctic and the "10-million-year flood". *Special Paper of the Geological Society of America*, *541*, 213–230. https://doi.org/10.1130/2018.2541(11)

Eren, M., Kadir, S., Kapur, S., Huggett, J., & Zucca, C. (2015). Colour origin of Tortonian red mudstones within the Mersin area, southern Turkey. *Sedimentary Geology*, *318*, 10–19.

Evans, J. E. (1991). Facies relationships, alluvial architecture, and paleohydrology of a Paleogene, humid- tropical alluvial-fan system; Chumstick formation, Washington state, USA. *Journal of Sedimentary Research*, *61*(5), 732–755.

Fordham, A. M., North, C. P., Hartley, A. J., Archer, S. G., & Warwick, G. L. (2010). Dominance of lateral over axial sedimentary fill in dryland rift basins. *Petroleum Geoscience*, *16*(3), 299–304.

Friedmann, S. J., & Burbank, D. W. (1995). Rift basins and supradetachment basins: Intracontinental extensional end-members. *Basin Research*, *7*(2), 109–127.

Gao, C., Ji, Y., Wu, C., Jin, J., Ren, Y., Yang, Z., Liu, D., Huan, Z., Duan, X., & Zhou, Y. (2020). Facies and depositional model of alluvial fan dominated by episodic flood events in arid conditions: An example from the quaternary poplar fan, North-Western China. *Sedimentology*, *67*(4), 1750–1796.

Garzanti, E., Padoan, M., Setti, M., López-Galindo, A., & Villa, I. M. (2014). Provenance versus weathering control on the composition of tropical river mud (southern Africa). *Chemical Geology*, *366*, 61–74.

Gawthorpe, R. L., & Leeder, M. R. (2000). Tectono-sedimentary evolution of active extensional basins. *Basin Research*, *12*(3–4), 195–218.

GeoRose 0.5.1. Yong Technology Inc. www.yongtechnology.com

Ghinassi, M., & Lelpi, A. (2018). Morphodynamics and facies architecture of streamflow-dominated, sand-rich alluvial fans, Pleistocene upper Valdarno Basin, Italy. *Geological Society, London, Special Publications*, *440*(1), 175–200.

Ghosh, P., Sarkar, S., & Maulik, P. (2006). Sedimentology of a muddy alluvial deposit: Triassic Denwa formation, India. *Sedimentary Geology*, *191*(1–2), 3–36.

Gnos, E. (1998). Peak metamorphic conditions of garnet amphibolites beneath the Semail ophiolite: Implications for an inverted pressure gradient. *International Geology Review*, *40*(4), 281–304.

Gray, D. R., Hand, M., Mawby, J., Armstrong, R. A., Miller, J. M., & Gregory, R. T. (2004). Sm–Nd and zircon U–Pb ages from garnet-bearing eclogites, NE Oman: Constraints on high-P metamorphism. *Earth and Planetary Science Letters*, *222*(2), 407–422.

Gulliford, A. R., Flint, S. S., & Hodgson, D. M. (2017). Crevasse splay processes and deposits in an ancient distributive fluvial system: The lower Beaufort group, South Africa. *Sedimentary Geology*, *358*, 1–18.

Hampton, B. A., & Horton, B. K. (2007). Sheetflow fluvial processes in a rapidly subsiding basin, Altiplano plateau, Bolivia. *Sedimentology*, *54*(5), 1121–1148.

Hansman, R. J., Ring, U., Thomson, S. N., Brok, B., & Stübner, K. (2017). Late Eocene uplift of the Al Hajar Mountains, Oman, supported by stratigraphy and low-temperature thermochronology. *Tectonics*, *36*, 3081–3109.

Harvey, A. M. (1997). The role of alluvial fans in arid-zone fluvial systems. In D. S. G. Thomas (Ed.), *Arid zone geomorphology; process, form and change in drylands* (2nd ed., pp. 231–259). Wiley.

Harvey, A. M., Mather, A. E., & Stokes, M. (2005). Alluvial fans: Geomorphology, sedimentology, dynamics—Introduction. A review of alluvial-fan research. *Geological Society, London, Special Publications*, *251*(1), 1–7.

Hein, F. J., & Walker, R. G. (1977). Bar evolution and development of stratification in the gravelly, braided, kicking Horse River, British Columbia. *Canadian Journal of Earth Sciences*, *14*(4), 562–570.

Hickson, T. A., Sheets, B. A., Paola, C., & Kelberer, M. (2005). Experimental test of tectonic controls on three-dimensional alluvial facies architecture. *Journal of Sedimentary Research*, *75*(4), 710–722.

High, L. R., & Picard, M. D. (1974). Reliability of cross-stratification types as paleocurrent indicators in fluvial rocks. *Journal of Sedimentary Research*, *44*(1), 158–168.

Hjellbakk, A. (1997). Facies and fluvial architecture of a high-energy braided river: The upper Proterozoic Seglodden member, Varanger peninsula, northern Norway. *Sedimentary Geology*, *114*(1–4), 131–161.

Horn, B. L. D., Goldberg, K., & Schultz, C. L. (2018). Interpretation of massive sandstones in ephemeral fluvial settings: A case study from the upper Candelária sequence (upper Triassic, Paraná Basin, Brazil). *Journal of South American Earth Sciences*, *81*, 108–121.

Huber, B. T., Norris, R. D., & MacLeod, K. G. (2002). Deep-sea paleotemperature record of extreme warmth during the cretaceous. *Geology*, *30*(2), 123–126.

Huerta, P., Armenteros, I., & Silva, P. G. (2011). Large-scale architecture in non-marine basins: The response to the interplay between accommodation space and sediment supply. *Sedimentology*, *58*(7), 1716–1736.

Jo, H. R., Rhee, C. W., & Chough, S. K. (1997). Distinctive characteristics of a streamflow-dominated alluvial fan deposit: Sanghori area, Kyongsang Basin (early cretaceous), southeastern Korea. *Sedimentary Geology*, *110*(1–2), 51–79.

Jones, B. G., & Rust, B. R. (1983). Massive sandstone facies in the Hawkesbury sandstone, a Triassic fluvial deposit near Sydney, Australia. *Journal of Sedimentary Research*, *53*(4), 1249–1259.

Jones, S. J., Frostick, L. E., & Astin, T. R. (2001). Braided stream and flood plain architecture: The Rio Vero formation, Spanish Pyrenees. *Sedimentary Geology*, *139*(3–4), 229–260.

Keller, G. (2004). Low-diversity, late Maastrichtian and early Danian planktic foraminiferal assemblages of the eastern Tethys. *The Journal of Foraminiferal Research*, *34*(1), 49–73.

Kraus, M. J. (1999). Paleosols in clastic sedimentary rocks: Their geologic applications. *Earth-Science Reviews*, *47*(1–2), 41–70.

Kumari, A., Singh, S., & Khosla, A. (2021). Palaeosols and palaeoclimate reconstruction of the Maastrichtian Lameta formation, Central India. *Cretaceous Research*, *117*, 104632.

Lecce, S. A. (1990). The alluvial fan problem. In *Alluvial fans: A field approach* (pp. 3–24).

Leeder, M. R., & Gawthorpe, R. L. (1987). Sedimentary models for extensional tilt-block/half-graben basins. *Geological Society, London, Special Publications*, *28*(1), 139–152.

Leleu, S., & Hartley, A. J. (2018). Constraints on synrift intrabasinal horst development from alluvial fan and aeolian deposits (Triassic, Fundy Basin, Nova Scotia). *Geological Society, London, Special Publications*, *440*(1), 79–101.

Levson, V. M., & Rutter, N. W. (2000). Influence of bedrock geology on sedimentation in pre-late Wisconsinan alluvial fans in the Canadian Rocky Mountains. *Quaternary International*, *68*, 133–146.

Lin, C., Liu, S., Tian, C., Zhuang, Q., Li, R., Tan, M., & Steel, R. J. (2022). Tectonic and climatic controls on the late Jurassic–early cretaceous stratigraphic architecture of the Xuanhua basin, North China. *Basin Research*, *34*(1), 190–219.

Mack, G. H., & Leeder, M. R. (1999). Climatic and tectonic controls on alluvial-fan and axial-fluvial sedimentation in the Plio-Pleistocene Palomas half graben, southern Rio Grande Rift. *Journal of Sedimentary Research*, *69*(3), 635–652.

Mack, G. H., & Rasmussen, K. A. (1984). Alluvial-fan sedimentation of the cutler formation (Permo-pennsylvanian) near gateway, Colorado. *Geological Society of America Bulletin*, *95*(1), 109–116.

Martinius, A. W., Elfenbein, C., & Keogh, K. J. (2014). Applying accommodation versus sediment supply ratio concepts to stratigraphic analysis and zonation of a fluvial reservoir. *From Depositional Systems to Sedimentary Successions on the Norwegian Continental Margin*, *46*, 101–125.

Mather, A. E., Harvey, A. M., & Stokes, M. (2000). Quantifying long-term catchment changes of alluvial fan systems. *Geological Society of America Bulletin*, *112*(12), 1825–1833.

Mather, A. E., Stokes, M., & Whitfield, E. (2017). River terraces and alluvial fans: The case for an integrated quaternary fluvial archive. *Quaternary Science Reviews*, *166*, 74–90.

Mattern, F., & Scharf, A. (2018). Postobductional extension along and within the frontal range of the eastern Oman Mountains. *Journal of Asian Earth Sciences*, *154*, 369–385.

Mattern, F., Scharf, A., Wang, P., Callegari, I., Abbasi, I., Al-Wahaibi, S., Pracejus, B., & Scharf, K. (2020). Deformation of the Cambro-Ordovician Amdeh formation (members 1 and 2): Characteristics, origins, and stratigraphic significance (Wadi Amdeh, Saih Hatat dome, Oman Mountains). *Geosciences*, *10*(2), 48.

Matthews, K. J., Maloney, K. T., Zahirovic, S., Williams, S. E., Seton, M., & Müller, R. D. (2016). Global plate boundary evolution and kinematics since the late Paleozoic. *Global and Planetary Change*, *146*, 226–250.

Miall, A. D. (1977a). A review of the braided-river depositional environment. *Earth-Science Reviews*, *13*(1), 1–62.

Miall, A. D. (1977b). Lithofacies types and vertical profile models in braided river deposits: A summary. In A. D. Miall (Ed.), *Fluvial Sedimentology* (pp. 597–604). Geological Survey of Canada.

Miall, A. D. (2010). Alluvial deposits. In N. P. James & R. W. Dalrymple (Eds.), *Facies models 4. Geological Association of Canada IV* (p. 6). Series: GEOtext.

Miall, A. D., & Jones, B. G. (2003). Fluvial architecture of the Hawkesbury sandstone (Triassic), near Sydney, Australia. *Journal of Sedimentary Research*, *73*(4), 531–545.

Miao, X., Lu, H., Li, Z., & Cao, G. (2008). Paleocurrent and fabric analyses of the imbricated fluvial gravel deposits in Huangshui Valley, the northeastern Tibetan plateau, China. *Geomorphology*, *99*(1–4), 433–442.

Mishra, S., Singh, S. P., Arif, M., Singh, A. K., Srivastava, G., Ramesh, B. R., & Prasad, V. (2022). Late Maastrichtian vegetation and palaeoclimate: Palynological inferences from the Deccan Volcanic Province of India. *Cretaceous Research*, *133*, 105126.

Moosdorf, N., Cohen, S., & von Hagke, C. (2018). A global erodibility index to represent sediment production potential of different rock types. *Applied Geography*, *101*, 36–44.

Moscariello, A. (2018). Alluvial fans and fluvial fans at the margins of continental sedimentary basins: Geomorphic and sedimentological distinction for geo-energy exploration and development. *Geological Society, London, Special Publications*, *440*(1), 215–243.

Nemec, W., & Muszyński, A. (1982). Volcaniclastic alluvial aprons in the tertiary of Sofia district (Bulgaria). *Annales Societatis Geologorum Poloniae*, *52*(1–4), 239–303.

Nemec, W., & Steel, R. J. (1984). Alluvial and coastal conglomerates: Their significant features and some comments on gravelly mass-flow deposits. *Sedimentology of gravels and conglomerates* (pp. 1–31). Canadian Society of Petroleum Geologists.

Nichols, G. J., & Fisher, J. A. (2007). Processes, facies and architecture of fluvial distributary system deposits. *Sedimentary Geology*, *195*(1–2), 75–90.

Nolan, S. C., Skelton, P. W., Clissold, B. P., & Smewing, J. D. (1990). Maastrichtian to early tertiary stratigraphy and palaeogeography

of the central and northern Oman Mountains. *Geological Society, London, Special Publications*, *49*(1), 495–519.

North, C. P., & Davidson, S. K. (2012). Unconfined alluvial flow processes: Recognition and interpretation of their deposits, and the significance for palaeogeographic reconstruction. *Earth-Science Reviews*, *111*(1–2), 199–223.

Nott, J. F., Thomas, M. F., & Price, D. M. (2001). Alluvial fans, landslides and late quaternary climatic change in the wet tropics of Northeast Queensland. *Australian Journal of Earth Sciences*, *48*(6), 875–882.

Nystuen, J. P., Kjemperud, A. V., Müller, R., Adestål, V., & Schomacker, E. R. (2014). Late Triassic to early Jurassic climatic change, northern North Sea region: Impact on alluvial architecture, palaeosols and clay mineralogy. In A. W. Martinius, R. Ravnås, J. A. Howell, R. J. Steel, & J. P. Wonham (Eds.), *From depositional systems to sedimentary successions on the Norwegian continental margin* (pp. 59–99). International Association of Sedimentologists.

Opluštil, S., & Vízdal, P. (1995). Pre-sedimentary palaeo-relief and compaction: Controls on peat deposition and clastic sedimentation in the Radnice member, Kladno Basin, Bohemia. *Geological Society, London, Special Publications*, *82*(1), 267–283.

Parker, G. (1999). Progress in the modeling of alluvial fans. *Journal of Hydraulic Research*, *37*(6), 805–825.

Peacock, D. C., & Sanderson, D. J. (1994). Geometry and development of relay ramps in normal fault systems. *AAPG Bulletin*, *78*(2), 147–165.

Prosser, S. (1993). Rift-related linked depositional systems and their seismic expression. *Geological Society, London, Special Publications*, *71*(1), 35–66.

Puy-Alquiza, M. J., Miranda-Avilés, R., García-Barragán, J. C., Loza-Aguirre, I., Li, Y., & Zanor, G. A. (2017). Facies analysis, stratigraphie architecture and depositional environments of the Guanajuato conglomerate in the sierra de Guanajuato, Mexico. *Boletín de la Sociedad Geológica Mexicana*, *69*(2), 385–408.

Reid, I., & Frostick, L. E. (1986). Dynamics of bedload transport in Turkey brook, a coarse-grained alluvial channel. *Earth Surface Processes and Landforms*, *11*(2), 143–155.

Renaut, R. W., & Gierlowski-Kordesch, E. H. (2010). Lakes. In N. P. James & R. W. Dalrymple (Eds.), *Facies models 4. Geological Association of Canada IV* (p. 6). Series: GEOtext.

Ridgway, K. D., & Decelles, P. G. (1993). Stream-dominated alluvial fan and lacustrine depositional systems in Cenozoic strike-slip basins, Denali fault system, Yukon territory, Canada. *Sedimentology*, *40*(4), 645–666.

Rogers, R. R., Kidwell, S. M., Deino, A. L., Mitchell, J. P., Nelson, K., & Thole, J. T. (2016). Age, correlation, and lithostratigraphic revision of the upper cretaceous (Campanian) Judith River formation in its type area (north-Central Montana), with a comparison of low-and high-accommodation alluvial records. *The Journal of Geology*, *124*(1), 99–135.

Rotevatn, A., Fossen, H., Hesthammer, J., Aas, T. E., & Howell, J. A. (2007). Are relay ramps conduits for fluid flow? Structural analysis of a relay ramp in arches National Park, Utah. *Geological Society, London, Special Publications*, *270*(1), 55–71.

Rotevatn, A., Jackson, C. A. L., Tvedt, A. B., Bell, R. E., & Blækkan, I. (2019). How do normal faults grow? *Journal of Structural Geology*, *125*, 174–184.

Rust, B. R. (1978). A classification of alluvial channel systems. In A. D. Miall (Ed.), *Fluvial sedimentology* (pp. 187–198). Canadian Society Petroleum Geologists Memoir.

Sadler, S. P., & Kelly, S. B. (1993). Fluvial processes and cyclicity in terminal fan deposits: An example from the late Devonian of Southwest Ireland. *Sedimentary Geology*, *85*(1–4), 375–386.

Saito, K., & Oguchi, T. (2005). Slope of alluvial fans in humid regions of Japan. *Taiwan and the Philippines. Geomorphology*, *70*(1–2), 147–162.

Schieber, J. (1999). Distribution and deposition of mudstone facies in the upper Devonian Sonyea Group of new York. *Journal of Sedimentary Research*, *69*(4), 909–925.

Schlische, R. W. (1995). Geometry and origin of fault-related folds in extensional settings. *AAPG Bulletin*, *79*(11), 1661–1678.

Schlische, R. W., Anders, M. H., & Beratan, K. K. (1996). Stratigraphic effects and tectonic implications of the growth of normal faults and extensional basins. *Special Papers-Geological Society Of America*, 183–203.

Schlüter, M., Steuber, T., Parente, M., & Mutterlose, J. (2008). Evolution of a Maastrichtian–Paleocene tropical shallow-water carbonate platform (Qalhat, NE Oman). *Facies*, *54*(4), 513–527.

Searle, M. (2019). *Geology of the Oman Mountains, eastern Arabia*. Springer.

Searle, M., & Cox, J. (1999). Tectonic setting, origin, and obduction of the Oman ophiolite. *Geological carpet Society of America Bulletin*, *111*(1), 104–122.

Searle, M. P. (2007). Structural geometry, style and timing of deformation in the Hawasina window, Al Jabal al Akhdar and Saih Hatat culminations, Oman Mountains. *GeoArabia*, *12*, 99–130.

Searle, M. P., & Cox, J. O. N. (2002). Subduction zone metamorphism during formation and emplacement of the Semail ophiolite in the Oman Mountains. *Geological Magazine*, *139*(3), 241–255.

Serck, C. S., & Braathen, A. (2019). Extensional fault and fold growth: Impact on accommodation evolution and sedimentary infill. *Basin Research*, *31*(5), 967–990.

Serck, C. S., Braathen, A., Olaussen, S., Osmundsen, P. T., Midtkandal, I., van Yperen, A. E., & Indrevær, K. (2021). Supradetachment to rift basin transition recorded in continental to marine deposition; Paleogene Bandar Jissah Basin, NE Oman. *Basin Research*, *33*(1), 544–569.

Sharp, J. M., Jr., Shi, M., & Galloway, W. E. (2003). Heterogeneity of fluvial systems—Control on density-driven flow and transport. *Environmental & Engineering Geoscience*, *9*(1), 5–17.

Siegenthaler, C., & Huggenberger, P. (1993). Pleistocene Rhine gravel: Deposits of a braided river system with dominant pool preservation. *Geological Society, London, Special Publications*, *75*(1), 147–162.

Smyrak-Sikora, A., Johannessen, E. P., Olaussen, S., Sandal, G., & Braathen, A. (2019). Sedimentary architecture during carboniferous rift initiation–the arid Billefjorden trough, Svalbard. *Journal of the Geological Society*, *176*(2), 225–252.

Smyrak-Sikora, A., Nicolaisen, J. B., Braathen, A., Johannessen, E. P., Olaussen, S., & Stemmerik, L. (2021). Impact of growth faults on mixed siliciclastic-carbonate-evaporite deposits during rift climax and reorganisation—Billefjorden trough, Svalbard, Norway. *Basin Research*, *33*(5), 2643–2674.

Smyrak-Sikora, A., Osmundsen, P. T., Braathen, A., Ogata, K., Anell, I., Mulrooney, M. J., & Zuchuat, V. (2020). Architecture of growth basins in a tidally influenced, prodelta to delta-front setting: The Triassic succession of Kvalpynten, East Svalbard. *Basin Research*, *32*(5), 949–978.

Sohn, Y. K. (1997). On traction-carpet sedimentation. *Journal of Sedimentary Research*, *67*(3), 502–509.

Sohn, Y. K., Rhee, C. W., & Kim, B. C. (1999). Debris flow and hyper-concentrated flood-flow deposits in an alluvial fan, northwestern part of the cretaceous Yongdong Basin, Central Korea. *The Journal of Geology*, *107*(1), 111–132.

Sønderholm, M., & Tirsgaard, H. (1998). Proterozoic fluvial styles: Response to changes in accommodation space (Rivieradal sandstones, eastern North Greenland). *Sedimentary Geology*, *120*(1–4), 257–274.

Steel, R., & Ryseth, A. (1990). The Triassic—Early Jurassic succession in the northern North Sea: Megasequence stratigraphy and intra-Triassic tectonics. *Geological Society, London, Special Publications*, *55*(1), 139–168.

Steel, R. J. (1993). Triassic–Jurassic megasequence stratigraphy in the Northern North Sea: Rift to post-rift evolution. *Geological Society of London*, *4*(1), 299–315.

Steel, R. J., Næhle, S., Nilsen, H., Røe, S. L., & Spinnangr, A. (1977). Coarsening-upward cycles in the alluvium of Hornelen Basin (Devonian) Norway: Sedimentary response to tectonic events. *Geological Society of America Bulletin*, *88*(8), 1124–1134.

Stikes, M. W. (2007). *Fluvial facies and architecture of the poison strip sandstone lower cretaceous Cedar Mountain formation, Grand County, Utah* (Vol. *6*). Utah Geological Survey.

Suresh, N., Bagati, T. N., Kumar, R., & Thakur, V. C. (2007). Evolution of quaternary alluvial fans and terraces in the intramontane Pinjaur dun, sub-Himalaya, NW India: Interaction between tectonics and climate change. *Sedimentology*, *54*(4), 809–833.

Tamura, A., & Arai, S. (2006). Harzburgite–dunite–orthopyroxenite suite as a record of supra-subduction zone setting for the Oman ophiolite mantle. *Lithos*, *90*(1–2), 43–56.

Terrizzano, C. M., Morabito, E. G., Christl, M., Likerman, J., Tobal, J., Yamin, M., & Zech, R. (2017). Climatic and tectonic forcing on alluvial fans in the southern Central Andes. *Quaternary Science Reviews*, *172*, 131–141.

Thorne, R., Roberts, S., & Herrington, R. (2012). The formation and evolution of the Bitincke nickel laterite deposit, Albania. *Mineralium Deposita*, *47*(8), 933–947.

Tucker, M. E. (2003). *Sedimentary rocks in the field*. John Wiley & Sons.

van de Kamp, P. C., & Leake, B. E. (1995). Petrology and geochemistry of siliciclastic rocks of mixed feldspathic and ophiolitic provenance in the northern Apennines, Italy. *Chemical Geology*, *122*(1–4), 1–20.

van Toorenenburg, K. A., Donselaar, M. E., & Weltje, G. J. (2018). The life cycle of crevasse splays as a key mechanism in the aggradation of alluvial ridges and river avulsion. *Earth Surface Processes and Landforms*, *43*(11), 2409–2420.

Villey, M., Le Métour, J., & de Gramont, X. (1986). *Geological map of Fanjah, sheet NF 40-3F, scale: 1:100,000, with explanatory notes*. Directorate General of Minerals, Oman Ministry of Petroleum and Minerals.

Viseras, C., & Fernández, J. (1994). Channel migration patterns and related sequences in some alluvial fan systems. *Sedimentary Geology*, *88*(3–4), 201–217.

Walsh, J. J., Watterson, J., Heath, A. E., & Childs, C. (1998). Representation and scaling of faults in fluid flow models. *Petroleum Geoscience*, *4*(3), 241–251.

Warren, C. J., & Waters, D. J. (2006). Oxidized eclogites and garnet-blueschists from Oman: P–T path modelling in the NCFMASHO system. *Journal of Metamorphic Geology*, *24*(9), 783–802.

Whiting, P. J., Dietrich, W. E., Leopold, L. B., Drake, T. G., & Shreve, R. L. (1988). Bedload sheets in heterogeneous sediment. *Geology*, *16*(2), 105–108.

Williams, R. M., Irwin, R. P., Zimbelman, J. R., Chidsey, T. C., & Eby, D. E. (2011). Field guide to exhumed paleochannels near Green River, Utah: Terrestrial analogs for sinuous ridges on Mars. *Analogs for Planetary Exploration*, *483*, 483–505.

Würtzen, C. L., Osmond, J. L., Faleide, J. I., Nystuen, J. P., Anell, I. M., & Midtkandal, I. (2022). Syn-to post-rift alluvial basin fill: Seismic stratigraphic analysis of Permian-Triassic deposition in the Horda platform, Norway. *Basin Research*, *34*(2), 883–912.

Zhang, L., Zhang, C., & Dou, L. (2021). Paleoenvironment implication of red Paleosols in a late cretaceous continental succession, Songliao Basin, NE China. *Minerals*, *11*(9), 993.